crystals

Review

Chemical Modifications of BDH-TTP [2,5-Bis(1,3-dithiolan-2-ylidene)-1,3,4,6-tetrathiapentalene]: Control of Electron Correlation

Jun-ichi Yamada * and Hiroki Akutsu

Department of Material Science, Graduate School of Material Science, University of Hyogo, 3-2-1 Kouto, Kamigori-cho, Ako-gun, Hyogo 678-1297, Japan; E-Mail: akutsu@sci.u-hyogo.ac.jp

* Author to whom correspondence should be addressed; E-Mail: yamada@sci.u-hyogo.ac.jp; Tel.: +81-791-58-0162; Fax: +81-791-58-0164.

Abstract: Organic molecular conductors with a strongly correlated electron system, in which the itinerancy of electrons (or holes) and the electron correlation (U/W, U, the on-site Coulomb repulsion, W, the bandwidth) compete with each other, are promising candidates for achieving superconductivity and also for exploring remarkable physical properties induced by external stimuli such as pressure, light, voltage and current. Our synthetic approach to the construction of strongly correlated organic electron systems is based on chemical modifications to the donor molecule BDH-TTP [2,5-bis(1,3-dithiolan-2-ylidene)-1,3,4,6-tetrathiapentalene] capable of producing metallic CT (charge-transfer) salts stable down to low temperatures (4.2–1.5 K). This aims at enhancing the electron correlation in the itinerant electron system by decreasing the bandwidth. Chemical modifications of BDH-TTP such as ring expansion of two outer dithiolane rings, replacement of one sulfur atom in an outer dithiolane ring with an oxygen atom and introduction of two methyl substituents into an outer ditiolane ring led to BDA-TTP [2,5-bis(1,3-dithian-2-ylidene)-1,3,4,6-tetrathiapentalene], DHOT-TTP [2-(1,3-dithiolan-2-ylidene)-5-(1,3-oxathiolan-2-ylidene)-1,3,4,6-tetrathiapentalene] and DMDH-TTP [2-(4,5-dimethyl-1,3-dithiolan-2-ylidene)-5-(1,3-dithiolan-2-ylidene)-1,3,4,6-tetrathiapentalene], respectively. In this review, the physical properties and the crystal and electronic structures of molecular conductors derived from these donor molecules will be described.

1. Introduction

Since the first example of metallic conductivity in a purely organic CT (charge-transfer) complex (TTF)(TCNQ) (TTF = tetrathiafulvalene, Figure 1; TCNQ = tetracyanoquinodimethane) [1] followed by the discovery of the first organic superconductor $(TMTSF)_2PF_6$ (TMTSF = tetramethyltetraselenafulvalene) [2], extensive studies on chemical modifications of the TTF donor molecule have been made to develop organic molecular conductors which show novel electrical conductivity, magnetism, optical properties and multifunctional properties combining conductivity (or even superconductivity) with magnetism [3–6]. Recently, notable physical phenomena such as a narrow gap (or zero-gap) conducting state [7], a photo-induced phase transition [8], a giant nonlinear resistance [9] and a current-induced metallic state [10], have been found in molecular conductors derived from TTF donors. These molecular conductors exhibit MI (metal-insulator) transitions with decreasing temperatures under ambient pressure. The phase transition from the metallic state with the itinerancy of electrons to the insulating state with the localized electrons is induced by enhancing the electron correlation, and hence the MI transition is characteristic of the strongly correlated electron system. Control of the electron correlation is also required for achieving organic superconductivity, as supported by the study of the phase diagram of BEDT-TTF [bis(ethylenedithio)tetrathiafulvalene] superconductors [11]. This study shows that the superconducting phase lies between the paramagnetic metallic phase and the antiferromagnetic insulating phase. Therefore, organic molecular conductors with the strongly correlated electron system have a great potential for leading to superconductivity as well as exotic physical properties induced by the application of external stimuli such as pressure, light, voltage and current.

Figure 1. Components of organic molecular conductors.
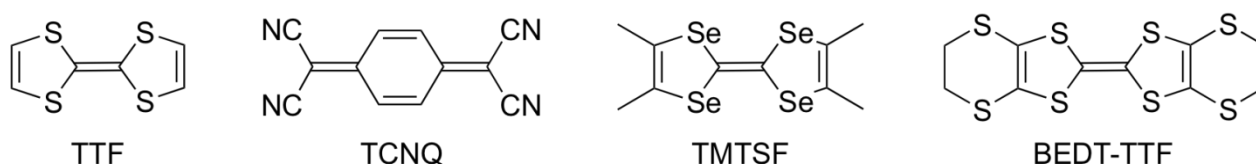
On the other hand, we have been studying the synthesis of donor molecules containing the BDY [bis(1,3-dithiol-2-ylidene), Figure 2a] unit as a π-electron system and the physical and structural properties of their CT materials [12–14]. Analogous to the TTF unit, the BDY unit consists of two DT (1,3-dithiol-2-ylidene) units; however, the linkage pattern of the two DT units in the BDY unit is different from that in the TTF unit. Accordingly, by comparing the physical and structural aspects of CT materials derived from the BDY donor family and the TTF donor family, a wider understanding of physical phenomena particular to organic molecular conductors would be gained. Among the BDY

donors we synthesized, BDH-TTP [2,5-bis(1,3-dithiolan-2-ylidene)-1,3,4,6-tetrathiapentalene] (Figure 2b) with various anions was found to form metallic salts stable down to low temperatures (4.2–1.5 K) [14,15], whereas BDA-TTP (Figure 2c) was found to produce ambient-pressure and pressure-induced superconductors [16–18]. Compared to the outer dithiolane rings of BDH-TTP, BDA-TTP has more expanded outer dithiane rings, so that the molecular structure of BDA-TTP is nonplanar in comparison with that of BDH-TTP. Such an extension of the σ bond framework from the five-membered ring to the six-membered ring results in steric hindrance of intermolecular interaction and, consequently, a decrease of the bandwidth. Therefore, unlike the stable metallic BDH-TTP salts regarded as an itinerant electron system, the electron correlation in BDA-TTP superconductors would be enhanced. In this way, chemical modifications of BDH-TTP to decrease the bandwidth would provide a synthetic avenue to new molecular conductors with a strongly correlated organic electron system.

Figure 2. **(a)** Bis(1,3-dithiol-2-ylidene) (BDY) unit. Molecular structures of **(b)** 2,5-bis(1,3-dithiolan-2-ylidene)-1,3,4,6-tetrathiapentalene (BDH-TTP) and **(c)** 2,5-bis(1,3-dithian-2-ylidene)-1,3,4,6-tetrathiapentalene (BDA-TTP).
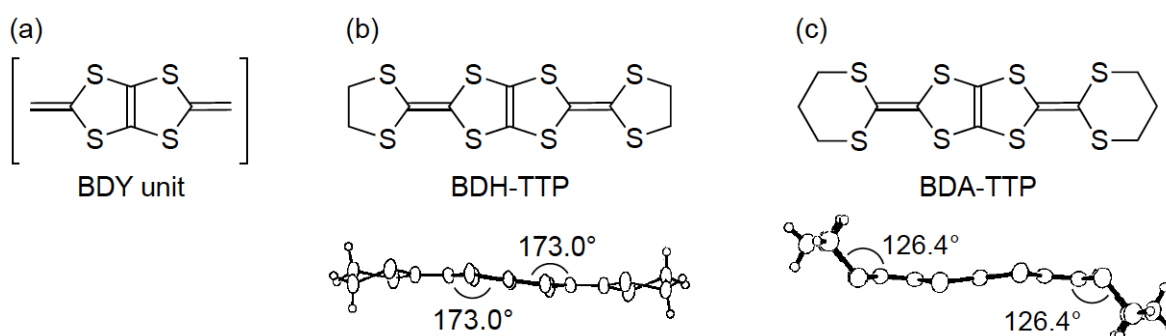

The emphasis of this review is first on our recent studies of the pressure-induced superconductor β-(BDA-TTP)$_2$I$_3$ and then on our chemical modifications to BDH-TTP for controlling the electron correlation.

2. Superconductivity in β-(BDA-TTP)$_2$I$_3$

Similar to BEDT-TTF, the π-electron donor BDA-TTP has the ability to give the ambient-pressure superconductors β-(BDA-TTP)$_2$X (X = SbF$_6$, AsF$_6$ and PF$_6$) [16] and the pressure-induced superconductors β-(BDA-TTP)$_2$MCl$_4$ (M = Ga and Fe) [17,18]. The structural feature common to BEDT-TTF and BDA-TTP in their charged states is a conformational flexibility originating from the outer six-membered rings. However, the pattern of conformational change in BDA-TTP is different from that in BEDT-TTP. It is known that there are two "twist" conformations, that is to say, the staggered and eclipsed conformations in the BEDT-TTF donor molecule (Figure 3a) [19]. On the other hand, a "flapping" motion of two terminal trimethylene (-CH$_2$CH$_2$CH$_2$-) groups of BDA-TTP with respect to the molecular plane including the π-electron system allows the outer dithiane rings to adopt various kinds of chair confirmations, which are divided broadly into two categories. The trimethylene end groups of BDA-TTP in β-(BDA-TTP)$_2$X (X = SbF$_6$, AsF$_6$ and PF$_6$) are found with opposite orientation with respect to the molecular plane (conformation A in Figure 3b): The same can be said for BDA-TTP in the neutral state (Figure 2c), whereas those in β-(BDA-TTP)$_2$MCl$_4$ (M = Ga and Fe)

are bonded to the molecular plane from the same side (conformation B in Figure 3b). It is therefore expected that, compared to the conformational change in BEDT-TTF by a "twisting" motion, the conformational change in BDA-TTP by a "flapping" motion is more sensitive to the applied pressure. This expectation prompted a study of the hydrostatic-pressure and uniaxial-strain effects on β-(BDA-TTP)$_2$I$_3$ [20,21].

Figure 3. Two main conformations of (**a**) bis(ethylenedithio)tetrathiafulvalene (BEDT-TTF) and (**b**) BDA-TTP in their charge-transfer (CT) materials.
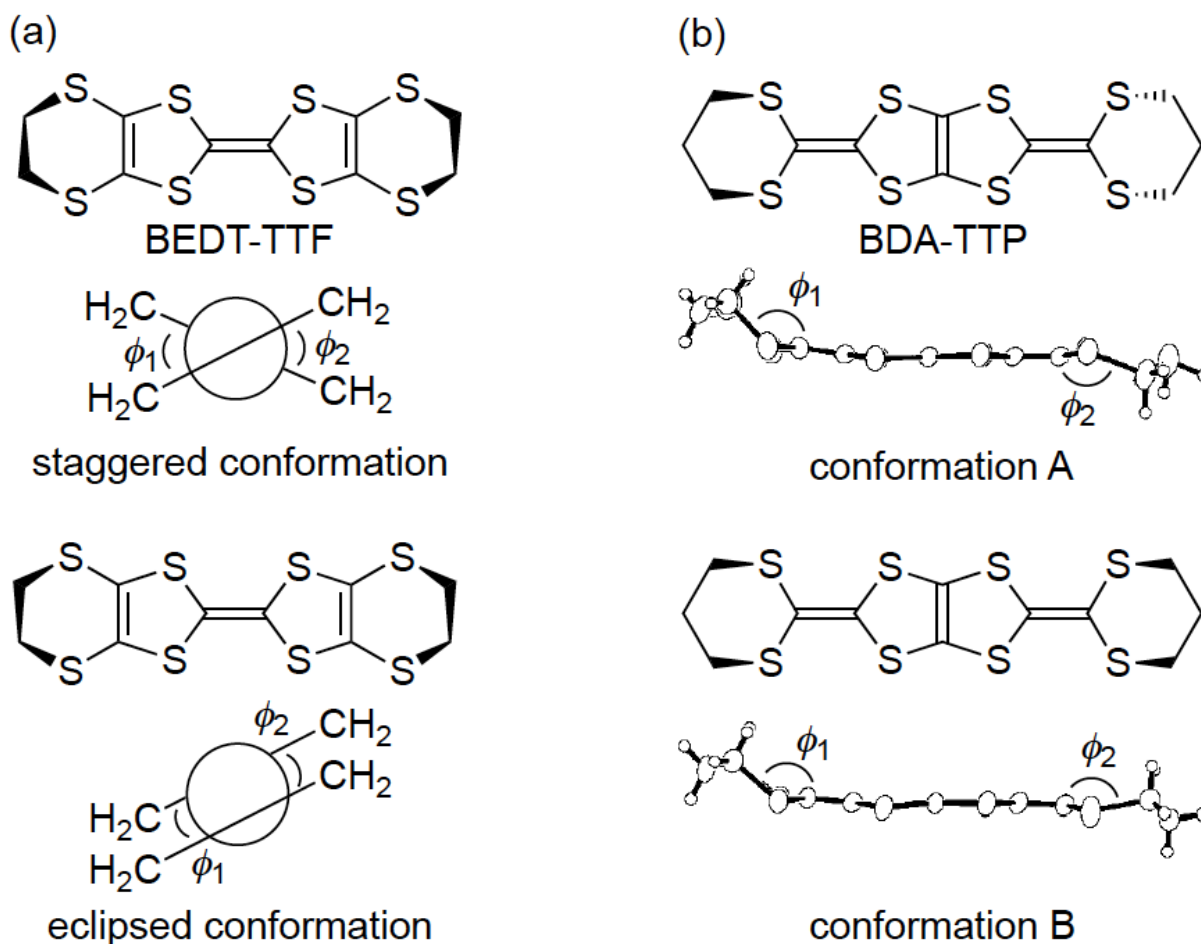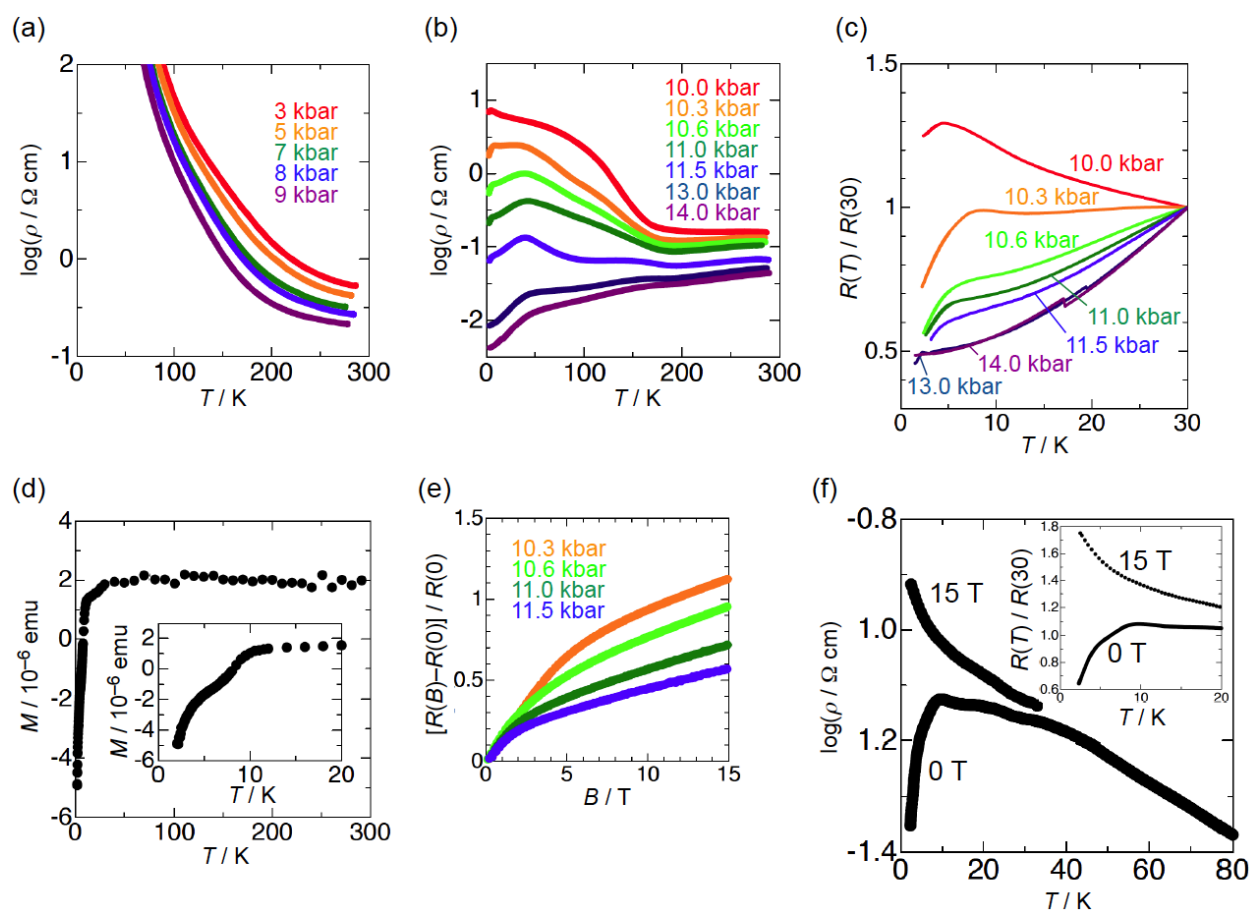

2.1. Effect of Hydrostatic Pressure

β-(BDA-TTP)$_2$I$_3$ at ambient pressure exhibited semiconducting behavior with E_a (activation energy) = 54 meV, and the temperature dependence of its susceptibility obeyed the 1D (one-dimensional) antiferromagnetic Heisenberg model (Figure 4). The susceptibility behavior implies a possibility of a pressure-induced superconductivity in β-(BDA-TTP)$_2$I$_3$, because the phase diagram of BEDT-TTF superconductors suggests the superconducting state lies adjacent to the antiferromagnetic insulating state, as mentioned above. Thus, hydrostatic-pressure experiments using β-(BDA-TTP)$_2$I$_3$ under up to 14 kbar were undertaken.

Figure 4. Temperature dependence of the susceptibility of β-(BDA-TTP)$_2$I$_3$. The dotted line represents a theoretical curve for the one-dimensional (1D) antiferromagnetic Heisenberg model with $J = -125(3)$ K (Reprinted with permission from reference 20, The Royal Society of Chemistry).
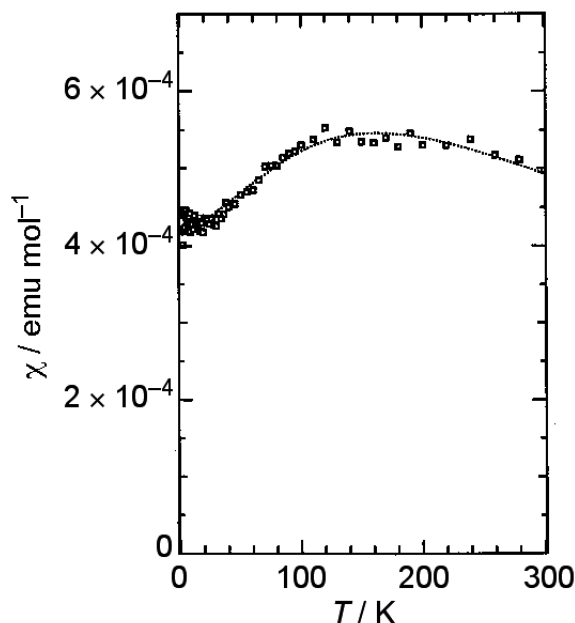
The semiconducting behavior of β-(BDA-TTP)$_2$I$_3$ observed at ambient pressure remained almost unaltered under pressures of up to 9 kbar (Figure 5a). To our surprise, a marked change in conductivity was found above 10 kbar (Figure 5b). At 10.0 kbar, the resistivity showed an almost temperature-independent value from room temperature, a change to semiconducting behavior below about 190 K and a drop with an onset at 4.5 K. In addition, the onset temperature of a resistivity drop reached 8.2 K by increasing the pressure by only 0.3 kbar (Figure 5c); however, with further increases in the pressure, it decreased slowly and no resistivity drop was observed at 14.0 kbar. To gain an insight as to whether the resistivity drop is attributable to a superconducting transition, we investigated a Meissner effect of this salt. As shown in Figure 5d, β-(BDA-TTP)$_2$I$_3$ under a magnetic field of 0.1 T at 10 kbar exhibited a sudden stepwise decrease in magnetization below 10.5 K. Furthermore, MR (magnetoresistance) measurements under pressures of 10.3 to 11.5 kbar at 1.6 K indicated that the resistance is restored by increasing the magnetic field (Figure 5e). Another sample at 9.7 kbar also showed a two-step resistivity drop with an onset at 9.5 K, which completely disappeared by applying a magnetic field of 15 T (Figure 5f). These results added to the superconductivity of β-(BDA-TTP)$_2$I$_3$. However, we failed to detect zero resistance in the salt probably due to a small volume fraction in the superconducting state observed.

Figure 5. Temperature dependence of the resistivity of β-(BDA-TTP)$_2$I$_3$ (**a**) under pressures of up to 9 kbar and (**b**) at different pressures 10.0, 10.3, 10.6, 11.0, 11.5, 13.0 and 14.0 kbar. (**c**) Temperature dependence of the relative resistance of β-(BAD-TTP)$_2$I$_3$ below 30 K under pressures of 10.0 to 14.0 kbar. (**d**) Temperature dependence of the magnetization of β-(BDA-TTP)$_2$I$_3$ under a magnetic field of 0.1 T at 10 kbar. The inset shows the magnetization below 20 K. (**e**) Magnetoresistance (MR) of β-(BDA-TTP)$_2$I$_3$ under different pressures 10.3, 10.6, 11.0 and 11.5 kbar at 1.6 K. (**f**) Magnetic field dependence of the resistance drop in β-(BDA-TTP)$_2$I$_3$ at 9.7 kbar. The inset shows the temperature dependence of the relative resistance below 20 K at 0 and 15 T (Reprinted with permission from reference 20, The Royal Society of Chemistry).

In order to elucidate the derivation of the structure-property relationship in β-(BDA-TTP)$_2$I$_3$, X-ray structural studies at ambient pressure and at a hydrostatic pressure of 7.5 kbar were carried out. The salt consists of alternate layers of BDA-TTP donor molecules arranged in the β-packing mode and layers of I$_3^-$ anions (Figure 6a). At ambient pressure, the BDA-TTP molecules in the donor layer are dimerized with interplanar distances of 3.65 and 3.49 Å to form a stack along the *a*-axis. Intermolecular chalcogen ··chalcogen contacts shorter than the sum of the van der Waals radii (or less than the van der Waals distance between chalcogen ··chalcogen atoms) are known to be important in studying the electronic structures of organic molecular conductors. In the case of β-(BDA-TTP)$_2$I$_3$, several S ··S contacts shorter than the van der Waals distance (3.70 Å) occur between donor stacks rather than within a donor stack (Figure 6b). The conformation of BDA-TTP donor molecules,

including the orientations of two trimethylene end groups with respect to the molecular plane, belongs to the same category as found in β-(BDA-TTP)$_2$X (X = SbF$_6$, AsF$_6$ and PF$_6$, conformation A in Figure 3b) and in the neutral structure of BDA-TTP (Figure 2c). At 7.5 kbar, the conformation of BDA-TTP is slightly different from that at ambient pressure (Figure 6c): The dihedral angles around the intramolecular sulfur-to-sulfur axes in two outer dithiane rings are 51.3° and 29.2°, respectively, whereas the corresponding dihedral angles at ambient pressure are 50.9° and 32.0°, respectively. To gain further information on the electronic structure of β-(BDA-TTP)$_2$I$_3$, we calculated the overlap integrals between the HOMO's (highest occupied molecular orbitals) of adjacent donor molecules by the extended Hückel method using the reported parameters [22] at ambient pressure and at 7.5 kbar (see the legend to Figure 6b). A comparison of the intrastack overlap integral ratio of $p1$ to $p2$ (2.73) at ambient pressure with the corresponding ratio (2.13) at 7.5 kbar indicates that the dimerization of donor molecules becomes small by applying pressure. However, the Fermi surface of β-(BDA-TTP)$_2$I$_3$ at 7.5 kbar, which was obtained by the tight-binding calculation method, is still open along the stacking a-axis (Figure 6d), similar to that at ambient pressure (Figure 6e). These open Fermi surfaces would be responsible for the semiconducting behavior of the salt observed under hydrostatic pressures ranging from ambient pressure to 9 kbar.

Figure 6. (**a**) Crystal structure of β-(BDA-TTP)$_2$I$_3$ at ambient pressure. Interplanar distances $d1$ and $d2$ are 3.65 and 3.49 Å, respectively (Reprinted with permission from reference 20, The Royal Society of Chemistry). (**b**) Donor arrangement in β-(BDA-TTP)$_2$I$_3$ at ambient pressure. Short S ··S contacts (< 3.70 Å) are shown by broken lines. Intermolecular overlap integrals $p1$, $p2$, c, $q1$ and $q2$ (× 10^{-3}) are 13.7 (15.7), 5.02 (7.36), −6.75 (−7.90), 0.20 (0.28) and −5.28 (−5.14), respectively; the corresponding values under a hydrostatic pressure of 7.5 kbar are shown in the parentheses (Reprinted with permission from reference 20, The Royal Society of Chemistry). (**c**) Molecular structure of BDA-TTP in β-(BDA-TTP)$_2$I$_3$ at 7.5 kbar. The dihedral angles $\varphi1$ and $\varphi2$ are 51.3°(50.9°) and 29.2°(32.0°), respectively; the corresponding angles at ambient pressure are shown in the parentheses (Reprinted with permission from reference 21, American Chemical Society). (**d**) Fermi surface of β-(BDA-TTP)$_2$I$_3$ at 7.5 kbar. (**e**) Fermi surface of β-(BDA-TTP)$_2$I$_3$ at ambient pressure (Reprinted with permission from reference 20, The Royal Society of Chemistry).
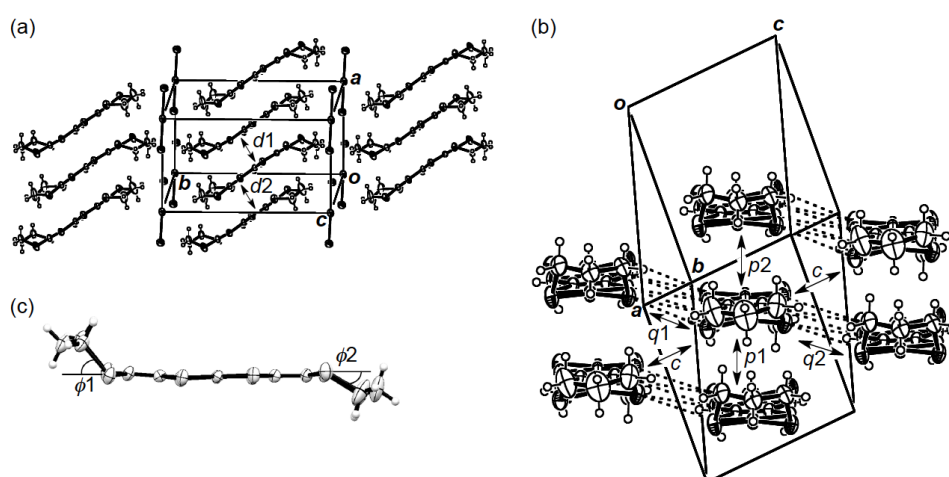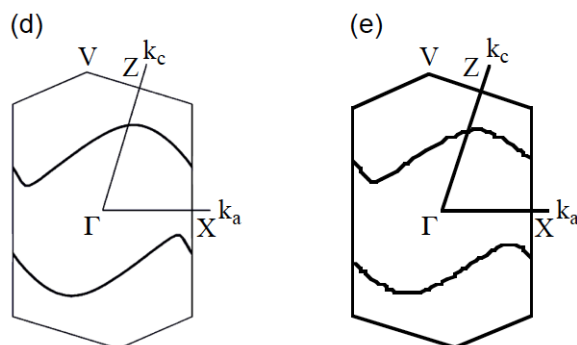
Figure 6. *Cont.*

2.2. Effect of Uniaxial Strain

On the basis of their band structures, organic superconductors fall into two main systems: The half-filled band system and the quarter-filled one [23]. In both systems, the T_c's (superconducting transition temperatures) are sensitive to pressure and the electronic states are also changed by pressure. In the case of many organic superconductors with the half-filled band system, with increasing pressure, the Mott insulating ground state is suppressed and then the superconducting state appears [24]. On the other hand, in the case of organic superconductors with the quarter-filled band system, the pressure enables the charge-ordered insulating state to change into the superconducting state [25,26]. Therefore, the application of pressure plays an important role in inducing organic superconductivity. In addition to the hydrostatic-pressure application with an isotropic pressure effect, the uniaxial-strain method with modification of the intermolecular distance along a desired direction is a powerful tool for the research of organic superconductors [27,28]. In this subsection, we address the following question: What changes take place in the T_c and P_c (critical superconducting pressure) of the pressure-induced superconductor β-(BDA-TTP)$_2$I$_3$ by making fine adjustments to the orientation of applying uniaxial strain. Before that, the electronic states and band structures of β-(BDA-TTP)$_2$I$_3$ at ambient pressure and at a hydrostatic pressure of 7.5 kbar are described.

The infrared and Raman spectroscopic study revealed that the BDA-TTP donor molecule in β-(BDA-TTP)$_2$I$_3$ is in the +0.5 oxidation state [29]. The result coupled with the susceptibility behavior explained by the 1D antiferromagnetic Heisenberg model (Figure 4) indicates that the ground state of β-(BDA-TTP)$_2$I$_3$ at ambient pressure is a Mott insulator with the half-filled band system, although there is an overlap between the upper and lower bands in the energy dispersion curve obtained by the tight-binding calculation using the extended Hückel method as shown in Figure 7a, where W, W_U and W_O stand for the total bandwidth of the upper and lower bands, the bandwidth of the upper band and the overlap between the upper and lower bands, respectively. The values of W and W_U are essential to the control of the effective electronic correlation, because the effective electronic correlation is given by U/W and V/W, where V is the intersite Coulomb repulsion, in the quarter-filled band system, and is expressed as U/W_U and V/W_U in the half-filled band system. Based on X-ray data of β-(BDA-TTP)$_2$I$_3$ at 7.5 kbar, it was found that the overlap W_O increases (Figure 7b) with a reduction of about 4% in the unit cell volume [917.2(11) Å^3] relative to that at ambient pressure [953.9(2) Å^3]. Therefore, the ground state of the salt is likely to change from the half-filled band into the quarter-filled one under applied pressure, because a large value of W_O is seen in the quarter-filled band structure [26].

Figure 7. Band structures of β-(BDA-TTP)$_2$I$_3$ (**a**) at ambient pressure and (**b**) at a hydrostatic pressure of 7.5 kbar. The values of W, W_U and W_O at ambient pressure are 0.65, 0.27 and 0.09 eV, respectively, whereas those at 7.5 kbar are 0.78, 0.36 and 0.15 eV, respectively (Reprinted with permission from reference 21, American Chemical Society).
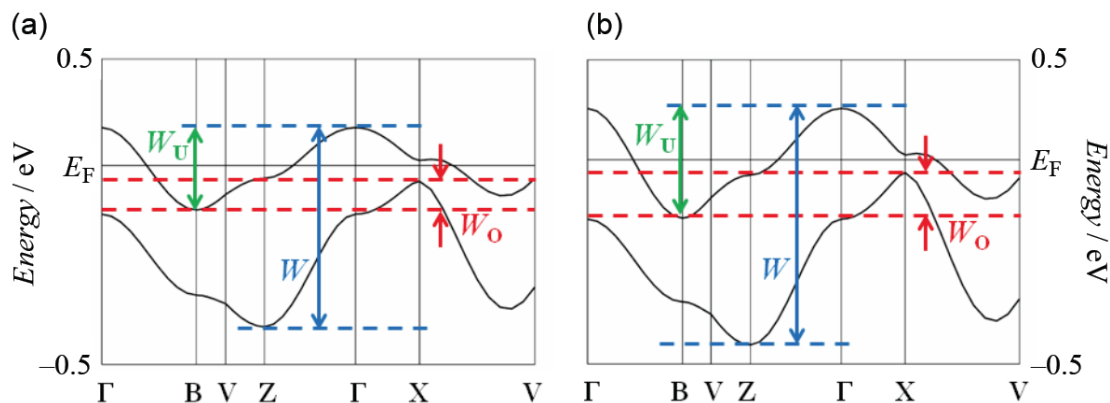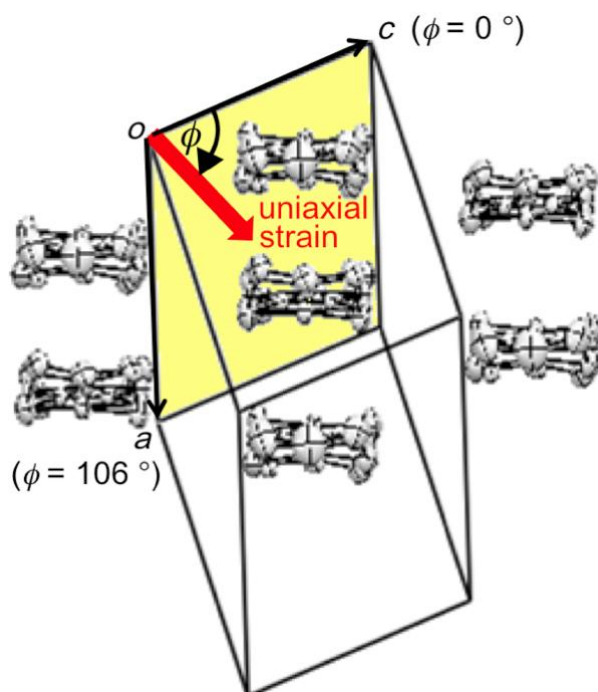

Figure 8. Definition of the orientation of uniaxial strain in the *ac* plane of β-(BDA-TTP)$_2$I$_3$. According to the definition, the orientations of the *c*-axis, *a*-axis and −*a*-axis strains are assigned by $\varphi = 0°$, 106° and −74°, respectively (Reprinted with permission from reference 21, American Chemical Society).

We investigated the temperature dependence of the resistivity of β-(BDA-TTP)$_2$I$_3$ by applying uniaxial strains along the crystallographic *a*-, *b*- and *c*-axes and then along different directions in the conducting *ac* plane to find favorable pressure orientations for inducing superconductivity. The orientation of uniaxial strain in the *ac* plane is defined by the angle φ from the *c*-axis fixed as a reference axis (Figure 8). Figure 9a–c shows the resistivity of the salt as a function of temperature under uniaxial strains parallel to the *a*-, *b*- and *c*-axes, respectively. Under the *a*-axis strains up to 12 kbar, increase of resistivity began to be suppressed in a low temperature region at 7, 8, 9 and

10 kbar, and the salt behaved like a metal from 50 to 10 K under 12 kbar. On the other hand, under the *b*-axis strains, the insulating behavior of the salt remained unchanged at all pressures up to 12 kbar. Under the *c*-axis strains up to 10 kbar, a drop in resistivity occurred with an onset at 8.5 K under 8.5 kbar. The onset temperature of the resistivity drop increased up to 10.5 K at 9.5 kbar, but decreased slightly to 9.5 K at 10 kbar. We observed a recovery of the resistance in the resistivity measurement of another single crystal by application of a uniaxal strain of 10 kbar with $\varphi = \sim7°$ under applied magnetic fields (Figure 9d); therefore, the drop in resistivity observed by applying the *c*-axis strain can be attributed to a superconducting transition. It was ultimately found that the maximum value of resistive T_c (abbreviated as T_{cmax}) under the *c*-axis strain rises by 1 K compared to that under hydrostatic pressure $(T_{cmax} = 9.5$ K).

Figure 9. Temperature dependence of the resistivity of β-(BDA-TTP)$_2$I$_3$ under the (**a**) *a*-axis, (**b**) *b*-axis and (**c**) *c*-axis strains. (**d**) Magnetic-field dependence of the resistivity drop in β-(BDA-TTP)$_2$I$_3$ under a uniaxial strain of 10 kbar with $\varphi = \sim7°$. The magnetic field was applied along the crystallographic *b*-axis (Reprinted with permission from reference 21, American Chemical Society).
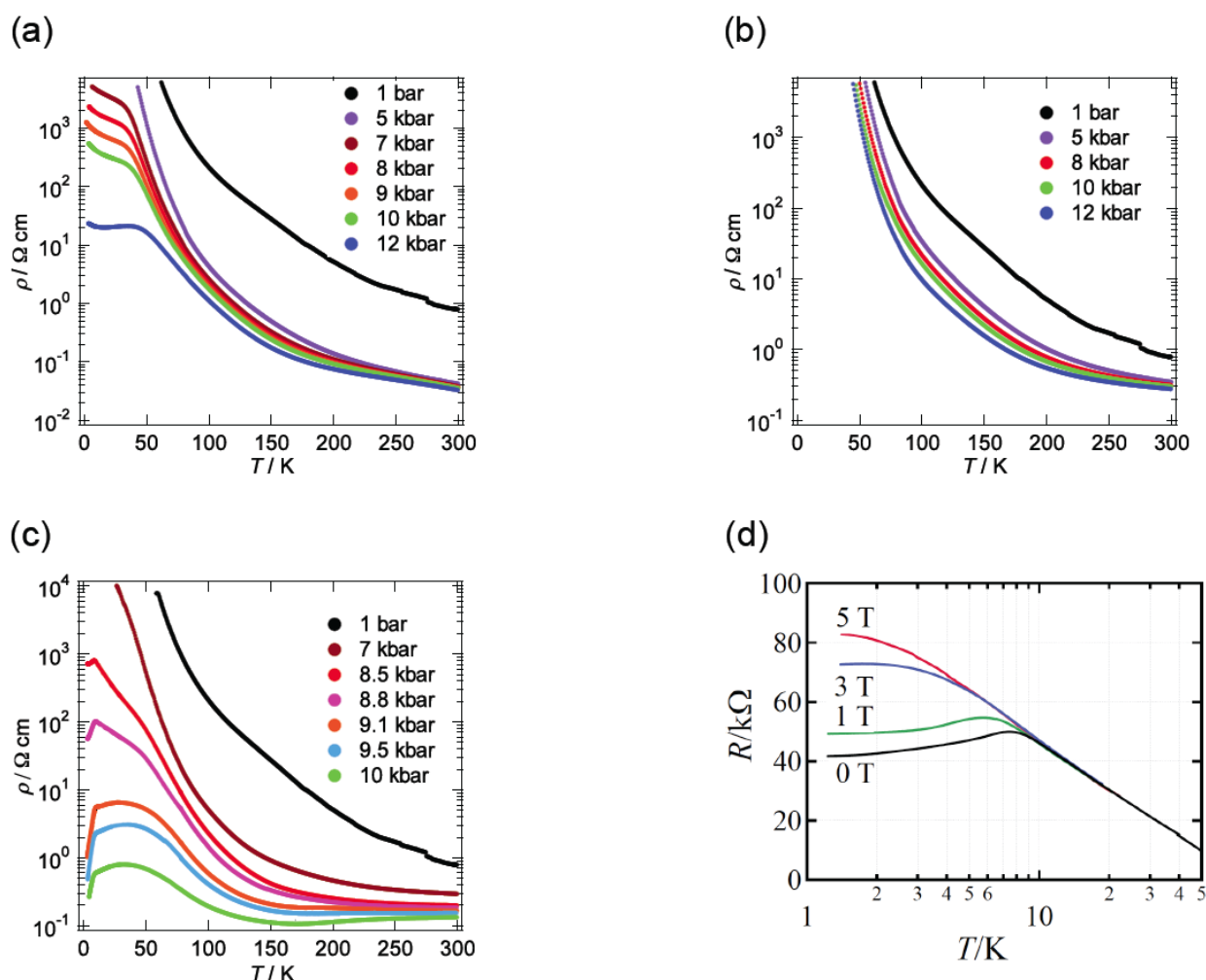

Figure 10a summarizes the pressure dependence of T_c in β-(BDA-TTP)$_2$I$_3$ by varying the orientation of uniaxial strain in the *ac* plane. Superconductivity was found in the orientation angle

range of $-47° \leq \varphi \leq 80°$; however, outside this range, no superconductivity was observed. It should be noted that at the uniaxial strain with $\varphi = 45°$, the T_c's varied from 4.3 to 10.3 K in a wide pressure range from 7 to 13.5 kbar and the P_c (7 kbar) is lower than that under hydrostatic pressure ($P_c = 9.7$ kbar). Figure 10b,c depicts the plots of the values of T_{cmax} and P_c, respectively, at different pressure orientations with $\varphi = -47°$, $-32°$, $-1°$, $16°$, $45°$, $58°$ and $80°$. Higher values of T_{cmax} from 8.5 to 10.5 K are recorded in the orientation angle range of $-32° \leq \varphi \leq 58°$, whereas the values of T_{cmax} decrease outside this range. The plots of P_c display a convex-shaped pressure-orientation dependence within the same orientation angle range ($-32° \leq \varphi \leq 58°$), outside which the values of P_c increase.

**Figure 10.** (**a**) Pressure dependence of T_c at different pressure orientations with $\varphi = -47°$, $-32°$, $-1°$, $16°$, $45°$, $58°$ and $80°$. Pressure-orientation dependences of (**b**) T_{cmax} and (**c**) P_c in β-(BDA-TTP)$_2$I$_3$ (Reprinted with permission from reference 21, American Chemical Society).
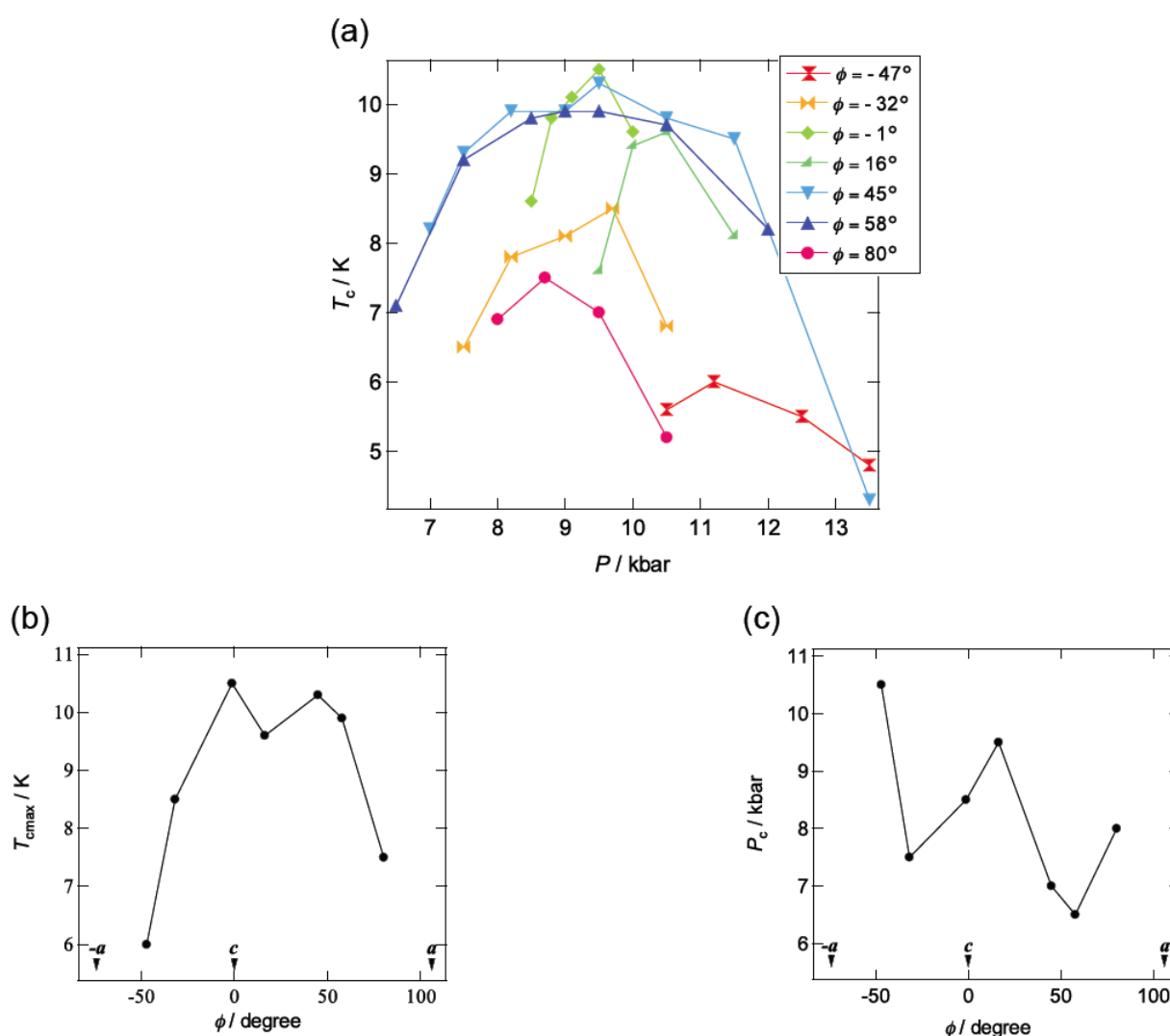
Taking account of the approximately 4% reduction of the unit cell volume by application of a hydrostatic pressure of 7.5 kbar, we calculated the tight-binding band structures under uniaxial strains parallel to the *ac* plane by the extended Hückel method based on the assumption that the distance between the BDA-TTP donor molecules along each uniaxial strain decreases by 5% with no change in

the HOMO level of BDA-TTP at ambient pressure. Figure 11 shows the curves of W, W_U and W_O, which were obtained from the band calculations by varying the pressure orientation angle at an interval of $5°$ in the *ac* plane, together with the values of W, W_U and W_O at ambient pressure. The value of W_O exhibits a gradual increase as φ approaches $0°$ (the direction of the *c*-axis), and a gradual decrease as φ come close to $106°$ (the direction of the *a*-axis) and $-74°$ (the direction of the –*a*-axis). A maximum value of W_O is observed at $\varphi = 16°$ (the direction perpendicular to the *a*-axis). The variation of W_O suggests that the ground state of β-(BDA-TTP)$_2$I$_3$ is changed from the half-filled band into the quarter-filled one by applying the *c*-axis strain, whereas the half-filled band is dominant in the ground state of β-(BDA-TTP)$_2$I$_3$ under the *a*-axis strain. It is noteworthy that compared to the value of W_O at ambient pressure, larger values of W_O are observed in the orientation angle range in which higher T_{cmax}'s are recorded (Figure 10b); therefore, the quarter-filled band system is likely to be favorable for the achievement of superconductivity in β-(BDA-TTP)$_2$I$_3$.

Figure 11. Pressure-orientation dependence of W, W_U and W_O in β-(BDA-TTP)$_2$I$_3$. The values of W, W_U and W_O at ambient pressure are indicated by the dotted lines (Reprinted with permission from reference 21, American Chemical Society).
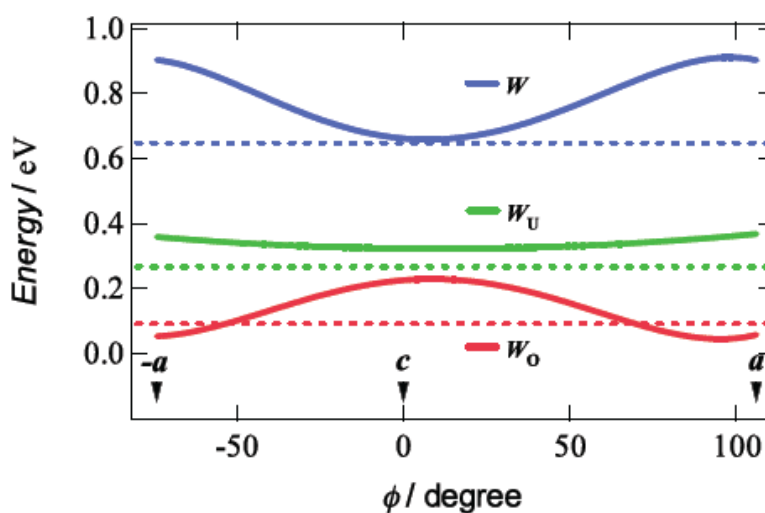
Application of pressure is generally thought to lead to an enhancement of the bandwidth and, consequently, to decrease the electron correlation [30]. In addition, a key parameter to control the ground state in the quarter-filled band system is proposed to be the effective electronic correlation U/W and V/W [23]. The ground state is in the metallic phase when the values of U/W and V/W are small, while the ground state is in the insulating phase when those are large. Superconductivity appears when U/W and V/W are in between. In the conducting *ac* plane of β-(BDA-TTP)$_2$I$_3$, the total bandwidth W under the *a*-axis strain exhibits a value close to the maximum (Figure 11), whereas the value of W at the uniaxial strain with $\varphi = 16°$ is minimal. With decreasing W, the values of U/W and V/W increase, so that the achievement of superconductivity requires an increase of pressure. It is thus predicted that the value of P_c shows a maximum around $\varphi = 16°$ and decreases as the orientation angle moves away from $\varphi = 16°$. This prediction is in good agreement with the pressure-orientation dependence of P_c in the orientation angle range of $-32° \leq \varphi \leq 58°$ (Figure 10c) where the ground state of β-(BDA-TTP)$_2$I$_3$ seems to be the quarter-filled band. At the pressure orientation angles of $-47°$ and $80°$, the ground

states are close to the half-filled band, the values of P_c significantly increase (Figure 10c) and the values of T_{cmax} decrease (Figure 10b).

The effective electronic correlation U/W_U and V/W_U in the half-filled band system acts as a key parameter to control the ground state [23], akin to the case of the quarter-filled band system. In the *ac* plane of β-(BDA-TTP)$_2$I$_3$, the values of the upper bandwidth W_U at different uniaxial strains are slightly larger than that at ambient pressure (Figure 11) and almost independent of φ. This pressure-orientation dependence of W_U differs from that of W. Thus it seems in the half-filled band system that a higher pressure is necessary for increase of W_U, and hence for decrease of U/W_U and V/W_U to induce superconductivity. As mentioned above, the ground state of β-(BDA-TTP)$_2$I$_3$ is regarded as the half-filled band for the pressure orientation along the *a*-axis, and we were actually unable to find superconductivity by applying the *a*-axis strains up to 12 kbar, though a metallic resistive behaviour as well as suppression of the resistivity increase were observed (Figure 9a). There is therefore a possibility that further increases in pressure along the *a*-axis achieve superconductivity in β-(BDA-TTP)$_2$I$_3$ with the half-filled band.

Our approach to the study of organic superconductivity described here, that is, the application of uniaxial strains with a variety of orientation angles demonstrates that the pressure orientation enables the ground state to change into another one, where the control of T_c is feasible by adjusting the intensity of uniaxial strain, considering the contribution of the effective electronic correlation. This work is thus the first example that realizes two competing insulating states depending on the pressure orientation in the same material, which is sure to shed light on the research of organic superconductors associated with those ground states. On the other hand, it remains to be proved that further application of the *a*-axis strain to β-(BDA-TTP)$_2$I$_3$ leads to superconductivity. Work currently in progress is addressing this issue.

3. DHOT-TTP Salts

The donor molecule BDH-TTP is a structural isomer of BEDT-TTF. It is well known that BEDT-TTF gives CT materials with a wide variety of electrical conducting properties, including insulators, semiconductors, metals and superconductors [3–6], whereas BDH-TTP shows the tendency to produce metallic CT salts with many anions [14,15,31–36]. The metallic conductivity observed in the BDH-TTP salts stems from a 2D (two-dimensional) interaction with a strong network of side-by-side, as well as face-to-face, S···S contacts shorter than the van der Waals distance (3.70 Å). The BDH-TTP molecule consists of two dithiolane rings and two dithiole rings (four five-membered ring systems). Thus, BDH-TTP is geometrically preferable to the BEDT-TTF molecule, which has two dihydrodithiin rings and two dithiole rings (two six-membered and two five-membered ring systems), for forming side-by-side S···S contacts, because four outer sulfur atoms in the dithiolane rings of BDH-TTP do not protrude from either side of the BDH-TTP molecule: An analogous geometrical difference can be found between BEDT-TTF and BDT-TTF [bis(1,3-dithiol-2-ylidene)-1,3,4,6-tetrathiapentalene] that is composed of four dithiole rings (four five-membered ring systems) and provides many metallic salts [37]. However, in order to control the electron correlation, the side-by-side S···S contacts caused by the BDH-TTP donor molecules should be reduced. A promising chemical modification in this regard is the substitution of one sulfur atom in the outer dithiolane ring

of BDH-TTP with an oxygen atom (which leads to DHOT-TTP [2-(1,3-dithiolan-2-ylidene)-5-(1,3-oxathiolan-2-ylidene)-1,3,4,6-tetrathiapentalene], Figure 12), because the incorporated oxygen atom would not easily participate in side-by-side chalcogen ··chalcogen contacts owing to its atomic radius shorter than that of sulfur. This chemical modification also means the introduction of two C–O bonds instead of two C–S bonds into the five-membered ring system with ring strain in BDH-TTP, which is expected to bring some distortion into the molecular structure due to the difference between the lengths of C–O and C–S bonds. Such a distortion would lead to a nonplanar structure in comparison with the molecular structure of BDH-TTP with planarity, and would cause a decrease in 2D interaction formed by the BDH-TTP donor molecules. The same chalcogen substitution in the outer dihydrodithiin ring of BEDT-TTF (which leads to ETOX [ethylenedithio(ethylenoxathio)tetrathiafulvalene]) has been reported [38]; however, no remarkable conformational difference between the molecular structures of BEDT-TTF and ETOX is discerned probably due to a structural flexibility of the six-membered ring system with less ring strain than the five-membered ring. Thus, to probe whether this subtle chemical modification of BDH-TTP gives rise to an appreciable conformational change in molecular structure and also to reveal what similarities and differences are found in the physical and structural properties of the DHOT-TTP and BDH-TTP salts, we undertook the synthesis of DHOT-TTP and the preparation of its CT salts [39,40].

Figure 12. Monooxgen-containing analogues of sulfur-based π-electron donors.
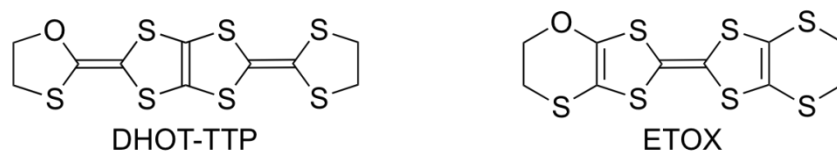
3.1. Synthesis, Molecular Structure and Electrochemical Properties of DHDO-TTP

We planned the synthesis of DHOT-TTP beginning with the oxathiolane-attached oxone **1a** (Figure 13). However, as previously reported by us [41], the preparation of **1a** from its dioxolane analogue **1b** results in a mixture of **1a,b** and the dithiolane-attached oxone **1c**. We thus examined the exclusive formation of **1a**. Treatment of **1b** with conc. H$_2$SO$_4$ in refluxing MeOH gave dimethyl acetal **2** in 72% yield, which upon heating with 2-mercaptoethanol in benzene containing a catalytic amount of *p*-TsOH led successfully to **1a** in 74% yield. Conversion of **1a** into the corresponding tin dithiolate **3** by sequential treatment with MeMgBr and Cl$_2$SnBu$_2$ in THF followed by reaction with 2-ethoxycarbonyl-1,3-dithiolane **4** in the presence of Me$_3$Al in CH$_2$Cl$_2$ gave the coupling product **5** in 39% overall yield. Subsequent oxidation of **5** with DDQ (2,3-dichloro-5,6-dicyano-1,4-benzoquinone) in refluxing toluene allowed the construction of DHOT-TTP in 88% yield.

According to structural information on DHOT-TTP in the neutral state, the DHOT-TTP molecules crystallize in an orientationally disordered manner with respect to the oxygen atom (O4 or O4′ in the atomic numbering scheme of Figure 14a) and the sulfur atom (S4 or S4′). In the molecular structure, the dihedral angles around the intramolecular sulfur-to-sulfur axes in two inner dithiole rings, hereafter defined as φ, are equivalently 152.2° (Figure 14b), which is smaller than the corresponding dihedral

angle (φ = 173 °, Figure 2b) in the BDH-TTP molecule. It is therefore clear that DHOT-TTP has a nonplanar structure compared to BDH-TTP.

Figure 13. Building blocks for the synthesis of 2-(1,3-dithiolan-2-ylidene)-5-(1,3-oxathiolan-2-ylidene)-1,3,4,6-tetrathiapentalene (DHOT-TTP).
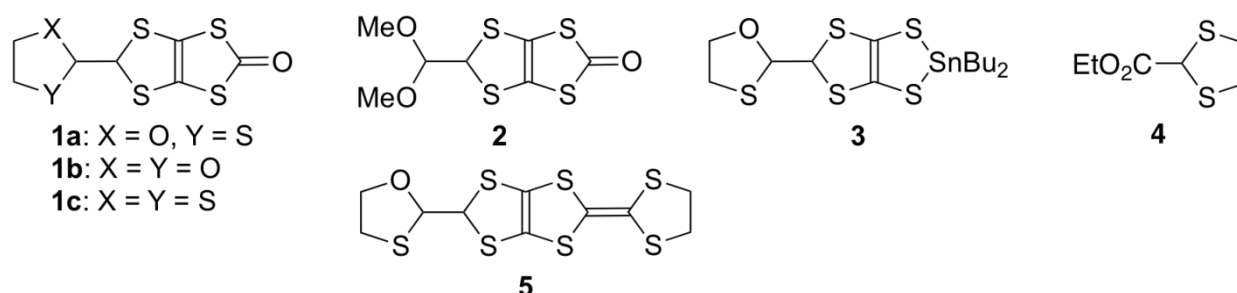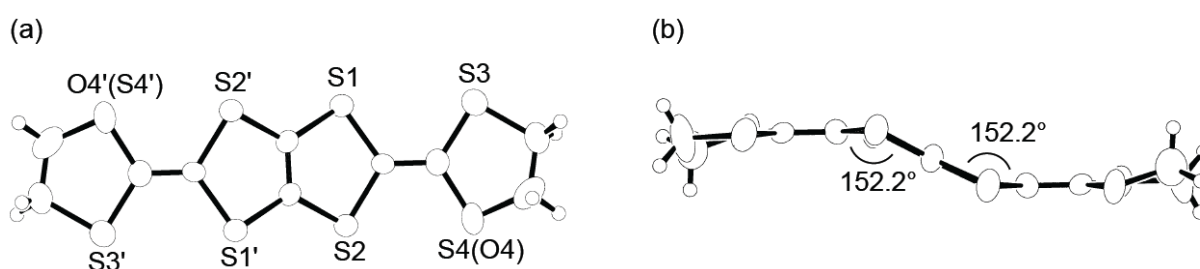

1a: X = O, Y = S
1b: X = Y = O
1c: X = Y = S

2

3

4

5

Figure 14. (**a**) Top and (**b**) side views of the molecular structure of DHOT-TTP (Reprinted with permission from reference 39, The Chemical Society of Japan).


CV (cyclic voltammetry) measurements of DHOT-TTP [E_1 = 0.52, E_2 = 0.80, E_3 = 1.16 V (*vs.* SCE)] and BDH-TTP [E_1 = 0.56, E_2 = 0.85, E_3 = 1.24, E_4 = 1.44 V (irreversible)] under identical conditions (0.1 M *n*-Bu$_4$NClO$_4$ in PhCN, Pt electrode, scan rate 50 mVs^{-1}) revealed that the E_1 value of DHOT-TTP is smaller than that of BDH-TTP and the ΔE ($E_2 - E_1$) value of DHOT-TTP (0.28 V) is almost equal to that of BDH-TTP (0.29 V). These results indicate that the replacement of one sulfur atom with oxygen slightly enhances the electron-donating ability, but scarcely affects the on-site Coulomb repulsion, similar to the electrochemical tendency found among BEDT-TTF and its oxygen-substituted analogues [38,42].

3.2. Physical Properties of DHDO-TTP Salts

In contrast to the metallic I$_3$ and BF$_4$ salts of BDH-TTP [15], DHOT-TTP gave the semiconducting I$_3$ and BF$_4$ salts with E_a = 17 and 45 meV, respectively [39]. In addition, the Au(CN)$_2$ salt of DHOT-TTP exhibited semiconducting behavior with E_a = 36 meV and σ_{rt} (room-temperature conductivity) = 2.4 S cm^{-1} [43]. The Au(CN)$_2{}^-$ anion with BDH-TTP also gave a semiconducting salt with E_a = 7 meV and σ_{rt} = 11 S cm^{-1} [43]; therefore, the Au(CN)$_2$ salt of BDH-TTP is an exception to the tendency that BDH-TTP forms metallic salts with linear, tetrahedral and octahedral anions [14]. On the other hand, as shown in Figure 15a, the resistivities of the AuI$_2$, PF$_6$ and AsF$_6$ salts of DHOT-TTP monotonically decreased with decreasing temperatures to 1.4 K: Similarities can be seen in the BDH-TTP salts with the same anions [15]. Variable-temperature resistivity measurement of the

FeCl$_4$ salt of DHOT-TTP showed some jumps in the cooling process and a large hump in the heating process (Figure 15b). The resistivity jumps are likely to be attributed to micro cracks caused by the stresses of the resistance-measuring probes. Furthermore, unlike κ-(BDH-TTP)$_2$FeCl$_4$ remaining metallic down to 1.5 K [31], a small upturn in resistivity was observed around 5 K. The magnetic susceptibility of the FeCl$_4$ salt of DHOT-TTP was fitted to a Curie–Weiss law from 2 to 300 K, giving a *C* (Curie constant) of 4.33 emu K mol^{-1} and a *θ* (Weiss constant) of −0.50 K. The fitted *C* is close to the value of 4.38 emu K mol^{-1} expected for a high-spin Fe^{3+} ion (*S* = 5/2, *g* = 2.0), thereby indicating that the Fe atom in the anion dominates the magnetization observed from 2 to 300 K. The small negative *θ* implies a very weak antiferromagnetic interaction between the Fe centers. Such a magnetic interaction, though very weak, does not occur in the paramagnetic κ-(BDH-TTP)$_2$FeCl$_4$ salt with *θ* = 0.041 K [31].

> **Figure 15.** Temperature dependence of the resitivities for the (**a**) AuI$_2$, PF$_6$, AsF$_6$ and (**b**) FeCl$_4$ salts of DHOT-TTP (Reprinted with permission from reference 40, The Chemical Society of Japan).
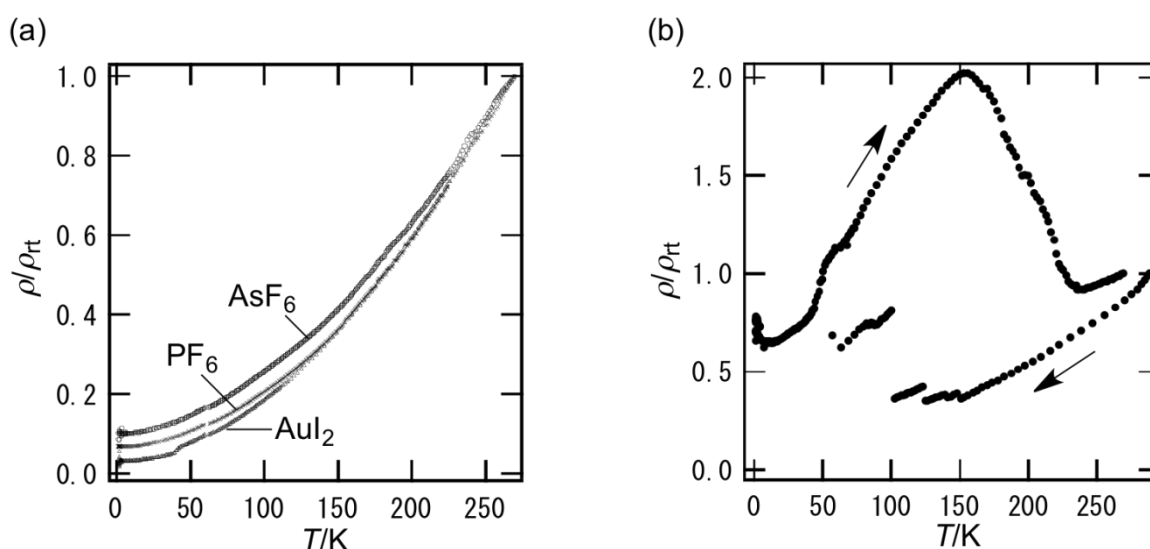
3.3. Structures of DHOT-TTP and BDH-TTP Salts with Linear Anions

While we were unable to obtain a single crystal of the semiconducting I$_3$ salt of DHOT-TTP suitable for an X-ray structural study, the stoichiometry and crystal structure of the metallic AuI$_2$ salt was determined by X-ray analysis [39]. The salt has a donor-to-anion ratio of 2:0.87 and consists of α-type donor layers alternating with anion layers (Figure 16a). In the donor layer, there are two crystallographically independent DHOT-TTP molecules, in one of which, unlike the neutral DHOT-TTP molecule, orientational disorder with respect to the oxygen atom is negligibly small within the accuracy of X-ray analysis. However, another independent DHOT-TTP molecule has orientational disorder between the oxygen and sulfur atoms in the oxathiolane ring: Occupancy factors for the oxygen sites are 0.62 and 0.38. The structures of both independent DHOT-TTP molecules take on planarity: The respective *φ*'s in the disorder-free DHOT-TTP molecule (molecule A) are 169.8 °and 175.2 °(Figure 17a), whereas those in the disordered DHOT-TTP molecule (molecule B) are 177.1 ° and 174.5 °(Figure 17b). DHOT-TTP donor molecules are stacked with some dimerization along the

c-axis to form two types of columns (columns A and B in Figure 16b). The interplanar distances in column A are 3.66 and 3.61 Å, whereas those in column B are 3.57 and 3.66 Å. The molecular plane of DHOT-TTP on column B is tilted by 50.1 ° from that on column A. Instead of no intermolecular S ··S contact shorter than the van der Waals distance (3.70 Å) within each column, there are several short S ··S contacts between columns A and B. Because of the orientational disorder between the oxygen and sulfur atoms in molecule B, the intermolecular overlap integrals were calculated by fixing the oxygen atom at the site with a larger occupancy factor (0.63). The absolute values of the overlap integrals between columns A and B (corresponding to $a1$, $a2$, $q1$ and $q2$) are all larger than those within both columns (corresponding to $c1$, $c2$, $c3$ and $c4$), reflecting the short S ··S contact pattern. The calculation result suggests a 2D interaction in the donor layer, which would be responsible for the metallic conductivity to 1.4 K.

Figure 16. (**a**) Crystal structure of α-(DHOT-TTP)$_2$(AuI$_2$)$_{0.87}$ viewed along the *a*-axis. (**b**) Donor arrangement in α-(DHOT-TTP)$_2$(AuI$_2$)$_{0.87}$. Interplanar distances in columns A and B are 3.66 (*d*1), 3.61 (*d*2), 3.57 (*d*3) and 3.66 (*d*4) Å, respectively. Short S ··S contacts (< 3.70 Å) are drawn by broken lines. Intermolecular overlap integrals $c1$, $c2$, $c3$, $c4$, $a1$, $a2$, $q1$ and $q2$ are −2.72, −1.86, −2.96, −0.26, −5.61, −7.56, 6.10 and 9.07×10^{-3}, respectively (Reprinted with permission from reference 39, The Chemical Society of Japan).
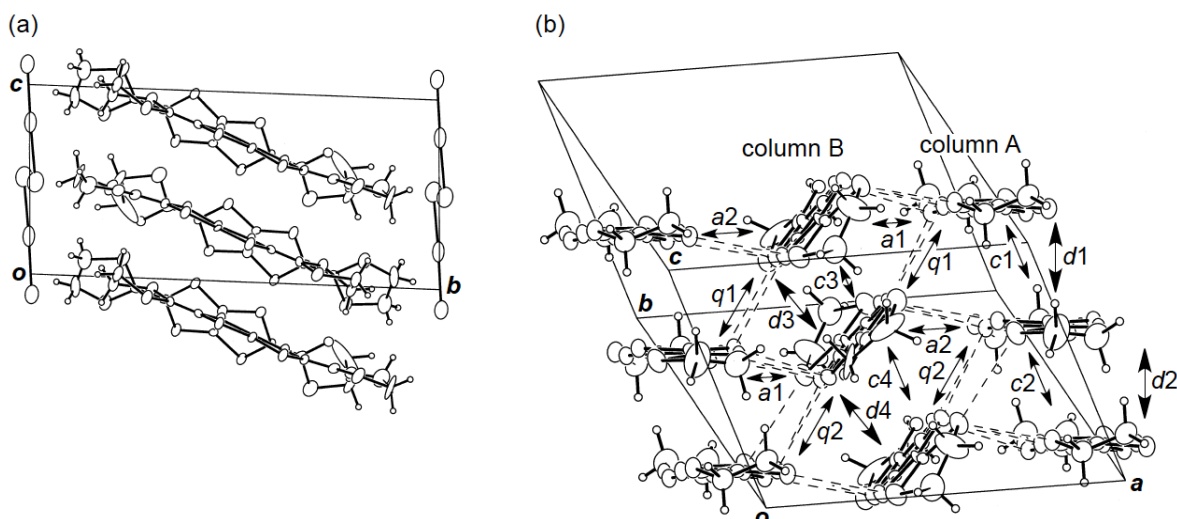

Figure 17. Side views of the structures of molecules (**a**) A and (**b**) B in α-(DHOT-TTP)$_2$(AuI$_2$)$_{0.87}$.

(a) 175.2° 169.8° molecule A (disorder-free)

(b) 174.5° 177.1° molecule B (with disorder)
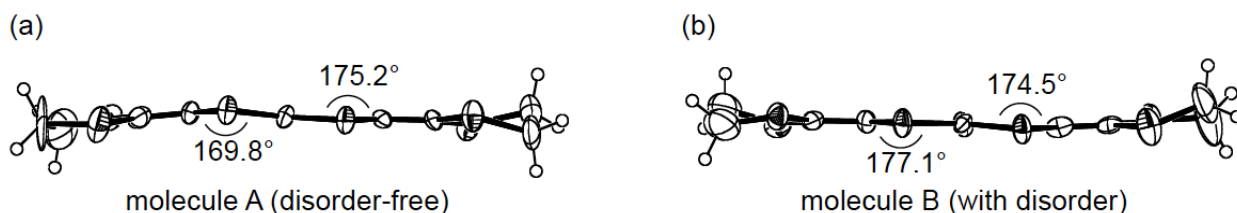
Since molecule A is free from disorder, its HOMO could be investigated by the extended Hückel method (Figure 18a). It should be noted that the coefficient of HOMO on the oxygen atom is considerably smaller than those on the sulfur atoms. Differences in the C–O and C–S bond lengths in

the oxathiolane ring can be also discerned (Figure 18b). The lengths of the two C–O bonds [C18–O2, 1.45(2) Å; C20–O2, 1.30(2) Å] are obviously shorter than those of the two C–S bonds [C18–S14, 1.74(1) Å; C19–S14, 1.82(2) Å]; nonetheless, molecule A lacks such nonplanarity as is seen in the molecular structure of DHOT-TTP in the neutral state (Figure 14b). This is probably because the central conjugated system of DHOT-TTP spreads out towards the outer chalcogen atoms with increasing charge, so that the distortion of molecular structure in the neutral state is relieved.

Figure 18. (**a**) Highest occupied molecular orbital (HOMO) and (**b**) ORTEP drawing of molecule A in α-(DHOT-TTP)$_2$(AuI$_2$)$_{0.87}$ (Reprinted with permission from reference 39, The Chemical Society of Japan).
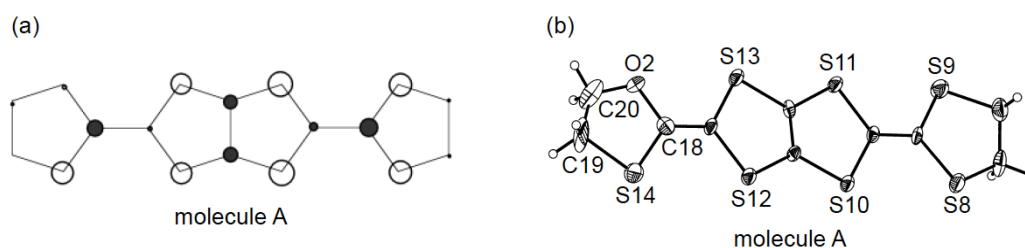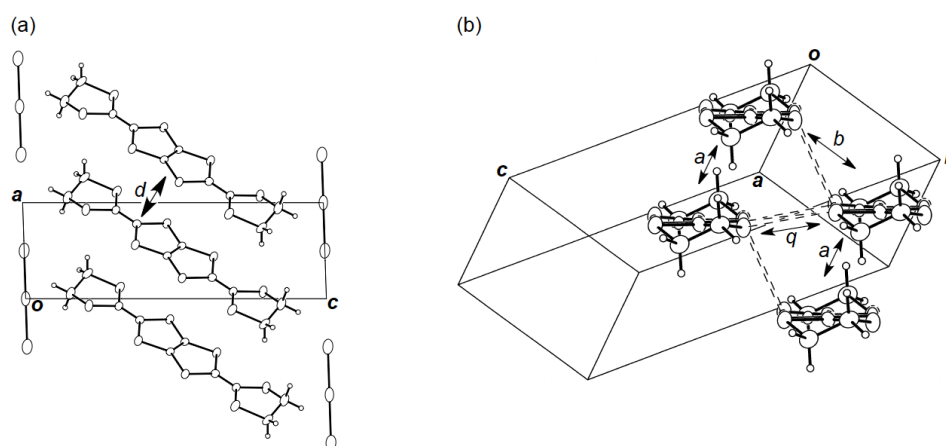

Figure 19. (**a**) Crystal structure of (BDH-TTP)$_2$AuI$_2$ viewed along the *b*-axis. Interplanar distance (*d*) is 3.63 Å. (**b**) Donor arrangement in (BDH-TTP)$_2$AuI$_2$. Short S ··S contacts (< 3.70 Å) are drawn by broken lines. Intermolecular overlap integrals *a*, *b* and *q* are 2.62, −14.5 and 9.21 × 10^{-3}, respectively.

Unlike the donor packing motif in α-(DHOT-TTP)$_2$(AuI$_2$)$_{0.87}$, the BDH-TTP donor molecules in the metallic (BDH-TTP)$_2$AuI$_2$ salt form a uniform stack with a constant interplanar spacing of 3.63 Å along the *a*-axis (Figure 19a) [43,44]. On the other hand, the S ··S contact pattern is similar to that observed in α-(DHOT-TTP)$_2$(AuI$_2$)$_{0.87}$: Short S ··S contacts are found between donor stacks rather than within a donor stack (Figure 19b). In addition, the absolute values of the interstack overlap integrals *b* and *q* are larger than that of the intrastack overlap integral *a*, which would lead to a 2D interaction responsible for the metallic state to 2.0 K. The planarity of BDH-TTP in (BDH-TTP)$_2$AuI$_2$ is somewhat enhanced (*φ* = 177.0, Figure 20a) compared to that of BDH-TTP in the neutral state (Figure 2b), and the distribution of its HOMO (Figure 20b) is quite similar to that of BDH-TTP in κ-(BDH-TTP)$_2$PF$_6$ [15]. Comparing the coefficients of HOMO of BDH-TTP in (BDH-TTP)$_2$AuI$_2$ with those of the disorder-free

DHOT-TTP molecule (molecule A, Figure 18a) in α-(DHOT-TTP)$_2$(AuI$_2$)$_{0.87}$, it is thought that the replacement of only one sulfur atom with oxygen in BDH-TTP corresponds just to the removal of the sulfur atom from BDH-TTP, and that the formation of a somewhat weak 2D interaction is possible. Actually, the largest absolute value of the interstack overlap integral in α-(DHOT-TTP)$_2$(AuI$_2$)$_{0.87}$ ($q2$ = 9.07 $\times$ 10^{-3}, Figure 16b) is less than two thirds of that in (BDH-TTP)$_2$AuI$_2$ (b = 14.5 $\times$ 10^{-3}, Figure 19b).

Figure 20. (**a**) Molecular structure and (**b**) HOMO of BDH-TTP in (BDH-TTP)$_2$AuI$_2$.
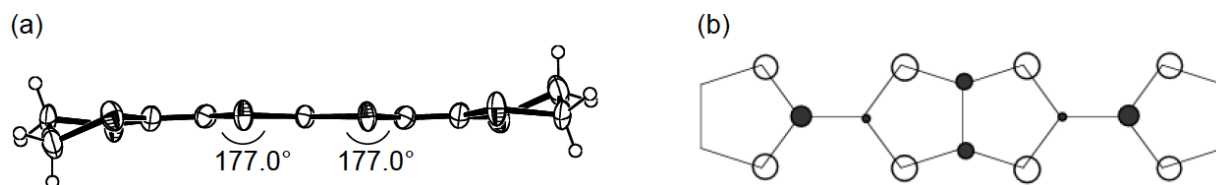
An additional comparative study of the structural aspects of DHOT-TTP and BDH-TTP salts was carried out with the semiconducting Au(CN)$_2$ salts of DHOT-TTP and BDH-TTP [43]. By X-ray analyses, both the crystal structures were found to be isostructural with each other and to consist of alternate layers of donor molecules arranged in the α-packing mode and layers of Au(CN)$_2^-$ anions [45,46]. Figure 21a shows the crystal structure of α-(DHOT-TTP)$_2$Au(CN)$_2$, in which the donor packing motif and the short S$\cdots$S contact pattern (Figure 21b) resemble those in α-(DHOT-TTP)$_2$(AuI$_2$)$_{0.87}$ (Figure 16b). The asymmetric unit contains two crystallographically independent donor molecules. These structural characteristics also hold for the α-(BDH-TTP)$_2$Au(CN)$_2$ salt. Figure 22a,b shows the ORTEP drawings of two independent DHOT-TTP donor molecules in α-(DHOT-TTP)$_2$Au((CN)$_2$: One (molecule C) has almost no orientational disorder for the oxygen atom, whereas the other (molecule D) has an orientational disorder among the oxygen atom and the three outer sulfur atoms in the oxathiolane and dithiolane rings: Occupancy factors for the oxygen sites are 0.15, 0.18, 0.23 and 0.44. The respective two dihedral angles φ's in molecules C and D are comparable to those in molecules A and B in α-(DHOT-TTP)$_2$(AuI$_2$)$_{0.87}$ (Figure 17a,b) and also to those in two independent BDH-TTP donor molecules (molecules E and F) in α-(BDH-TTP)$_2$Au(CN)$_2$ (Figure 23a,b). Two ethylene carbon atoms on one side in molecule E have thermal disorder (Figure 23a). The distribution of HOMO in the disorder-free molecule C (Figure 22c) is almost the same as that in the disorder-free molecule A in α-(DHOT-TTP)$_2$(AuI$_2$)$_{0.87}$ (Figure 18a). In the donor layers of both α-(DHOT-TTP)$_2$Au(CN)$_2$ and α-(BDH-TTP)$_2$Au(CN)$_2$, the dihedral angles between the molecular planes of π-donors on neighboring stacks are 50.2$°$ and 44.9$°$, respectively, and the absolute values of the intrastack overlap integrals $c1$, $c2$, $c3$ and $c4$, which were calculated by fixing the oxygen atom at the site with the largest occupancy factor (0.44) in the disordered molecule D in the case of α-(DHOT-TTP)$_2$Au(CN)$_2$, are smaller than those of the interstack overlap integrals $a1$, $a2$, $q1$ and $q2$ (Figure 21b). In particular, a very small value and relatively small values are estimated for the intrastack overlap integral $c1$ (0.08 $\times$ 10^{-3}) in α-(DHOT-TTP)$_2$Au(CN)$_2$ and for the intrastack overlap integrals $c2$ and $c4$ (0.37 and 0.75 $\times$ 10^{-3}) in α-(BDH-TTP)$_2$Au(CN)$_2$, respectively, which would be responsible for the semiconducting behaviors of both salts. Comparing the absolute values of the interstack overlap integrals in both salts, no remarkable differences in the $a1$ and $q1$ values [6.47 and

9.20×10^{-3} in α-(DHOT-TTP)$_2$Au(CN)$_2$; 5.67 and 9.34×10^{-3} in α-(BDH-TTP)$_2$Au(CN)$_2$] are found, whereas the $a2$ and $q2$ values in α-(DHOT-TTP)$_2$Au(CN)$_2$ (5.44 and 6.65×10^{-3}) are smaller than those in α-(BDH-TTP)$_2$Au(CN)$_2$ (8.38 and 10.7×10^{-3}). Therefore, it appears that the side-by-side interaction between donor molecules is somewhat weakened by introducing the oxygen atom instead of the sulfur atom.

Figure 21. (**a**) Crystal structures of α-(DHOT-TTP)$_2$Au(CN)$_2$ viewed along the *a*-axis. (**b**) Donor arrangement in α-(DHOT-TTP)$_2$Au(CN)$_2$. Interplanar distances are 3.68 (*d1*), 3.62 (*d2*), 3.65 (*d3*) and 3.62 (*d4*) Å, whereas those in α-(BDH-TTP)$_2$Au(CN)$_2$ are 3.78 (*d1*), 3.67 (*d2*), 3.66 (*d3*) and 3.63 (*d4*) Å. Short S $\cdot\cdot$S contacts (< 3.70 Å) are drawn by dotted lines. The values of intermolecular overlap integrals *c1*, *c2*, *c3*, *c4*, *a1*, *a2*, *q1* and *q2* are 0.08, −2.55, −1.94, −3.63, 6.47, 5.44, −9.20 and -6.65×10^{-3}, respectively, whereas the corresponding values in α-(BDH-TTP)$_2$Au(CN)$_2$ are 3.99 (*c1*), 0.37 (*c2*), −2.94 (*c3*), −0.75 (*c4*), 5.67 (*a1*), 8.38 (*a2*), −9.34 (*q1*) and −10.7 (*q2*) $\times 10^{-3}$.
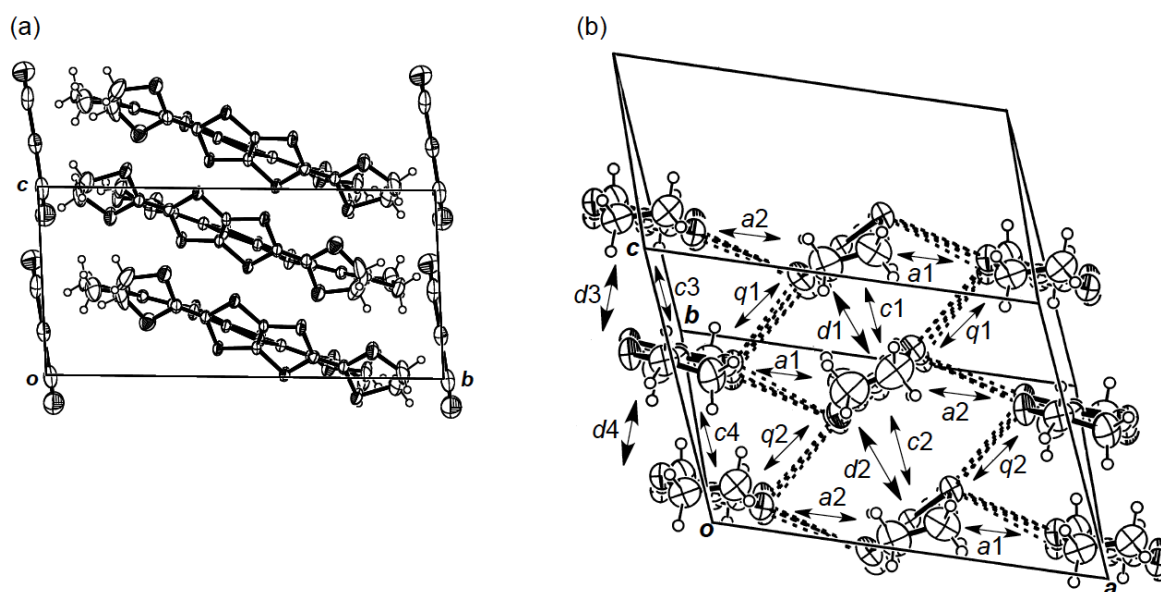
Figure 22. Structures of molecules (**a**) C and (**b**) D in α-(DHOT-TTP)$_2$Au(CN)$_2$. (**c**) HOMO of molecule C.
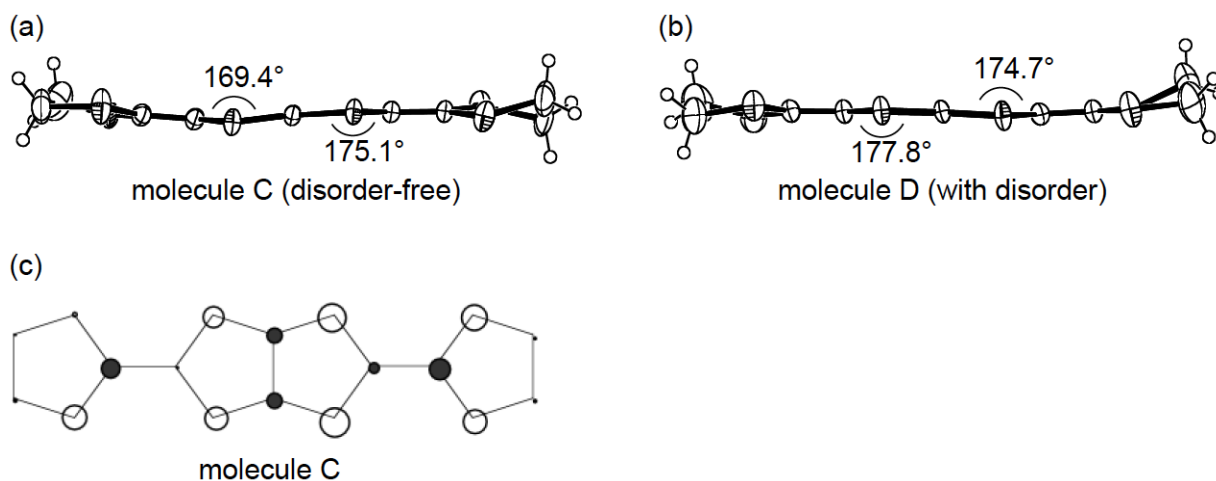
Figure 23. Structures of two independent BDH-TTP molecules (**a**) E and (**b**) F in α-(BDH-TTP)$_2$Au(CN)$_2$.

(a)

171.1°

174.9°

molecule E

(b)

174.1°

176.0°

molecule F
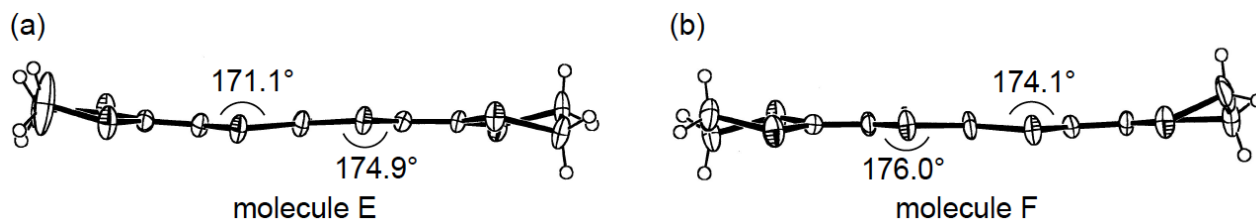
3.4. Structures of κ-Type DHOT-TTP Salts

As mentioned above, α-type donor packing motifs occurred in the AuI$_2$ and Au(CN)$_2$ salts of DHDO-TTP. On the other hand, DHOT-TTP with the PF$_6^-$, AsF$_6^-$ and FeCl$_4^-$ anions formed CT salts with κ-type donor packing motifs [40], the structures of which are described in this subsection.

Figure 24. (**a**) Donor arrangement in κ-(DHOT-TTP)$_2$PF$_6$. Broken lines indicate short S ··S contacts (< 3.70 Å). The respective values of overlap integrals *p*1, *p*2, *q*1 and *q*2 are 20.5, 22.3, 6.22 and −5.07 × 10^{-3}, whereas those in κ-(DHOT-TTP)$_2$AsF$_6$ are 20.1, 22.3, 6.36 and −4.97 × 10^{-3}. (**b**) Donor arrangement in κ-(DHOT-TTP)$_2$FeCl$_4$. Broken lines indicate short S ··S contacts (<3.70 Å). The respective values of overlap integrals *p*1, *p*2, *q*1 and *q*2 are 17.8, 17.9, 6.24 and −4.65, respectively (Reprinted with permission from reference 40, The Chemical Society of Japan).

(a)

(b)
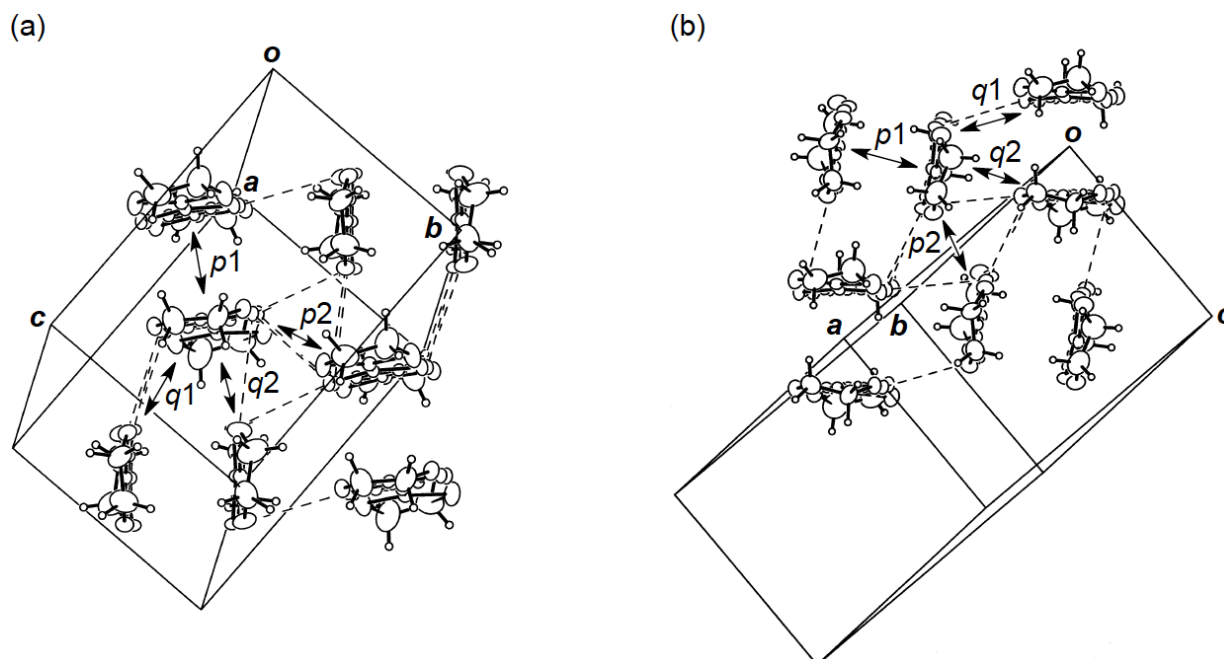
X-ray structural studies of the PF$_6$ and AsF$_6$ salts of DHOT-TTP established that both salts crystallize isostructurally and, additionally, are isostructural to κ-(BDH-TTP)$_2$PF$_6$ [15]. Figure 24a shows the donor packing motif of κ-(DHOT-TTP)$_2$PF$_6$, in which the DHOT-TTP molecule has orientational disorder among four outer chalcogen atoms in the oxathiolane and dithiolane rings: Occupancy factors for the oxygen sites are 0.28, 0.27, 0.23 and 0.22. There are several short S ··S

contacts (less than the van der Waals distance of 3.70 Å) between donor pairs, whereas no short $S \cdots S$ contact is observed within a donor pair. The $S \cdots S$ contact pattern is somewhat different from that observed in κ-(BDH-TTP)$_2$PF$_6$, in which each BDH-TTP donor molecule is linked by short intrapair and interpair $S \cdots S$ contacts. Intermolecular overlap integrals were calculated by fixing the oxygen atom at the site with the largest occupancy factor (0.28). According to the extended Hückel calculation, the coefficient of HOMO on the fixed oxygen atom in DHOT-TTP is very small, close to those on the oxygen atoms in the disorder-free DHOT-TTP molecules, molecule A (Figure 18a) in α-(DHOT-TTP)$_2$(AuI$_2$)$_{0.87}$ and molecule C (Figure 22c) in α-(DHOT-TTP)$_2$Au(CN)$_2$. Despite no short intrapair $S \cdots S$ contact, large values of the intermolecular overlap integrals are found within a donor pair ($p1 = 20.5 \times 10^{-3}$) as well as between donor pairs ($p2 = 22.3 \times 10^{-3}$). Compared to the corresponding values of intrapair and interpair overlap integrals in κ-(BDH-TTP)$_2$PF$_6$ (20.7 and 19.6×10^{-3} [15]), the $p1$ value is almost equal and the $p2$ value is slightly large: The same is true of κ-(DHOT-TTP)$_2$AsF$_6$ ($p1 = 20.1 \times 10^{-3}$, $p2 = 22.3 \times 10^{-3}$). Therefore, similar to κ-(BDH-TTP)$_2$PF$_6$, κ-(DHOT-TTP)$_2$X (X = PF$_6$ and AsF$_6$) are regarded as 2D metals, and hence would remain metallic all the way down to 1.4 K.

Analogous to an isostructural series of κ-(DHOT-TTP)$_2$X (X = PF$_6$ and AsF$_6$) and κ-(BDH-TTP)$_2$PF$_6$, the structure of the FeCl$_4$ of DHOT-TTP was found by X-ray analysis to be isostructural to κ-(BDH-TTP)$_2$FeCl$_4$ [31]. Figure 24b shows the donor arrangement of κ-(DHOT-TTP)$_2$FeCl$_4$. The oxygen atom of the DHOT-TTP molecule in the salt is orientationally disordered with the three outer sulfur atoms in the oxathiolane and dithiolane rings: Occupancy factors for the oxygen sites are 0.37, 0.36, 0.19 and 0.08. As is the case in κ-(BDH-TTP)$_2$FeCl$_4$, short $S \cdots S$ contacts are observed between donor pairs, but not within a donor pair. Nevertheless, calculation of the intermolecular overlap integrals by fixing the oxygen atom at the site with the largest occupancy factor (0.37) revealed that the value of the intrapair overlap integral $p1$ (17.8×10^{-3}) is almost equal to the largest value ($p2 = 17.9 \times 10^{-3}$) among the interpair overlap integrals. Although the $p1$ and $p2$ values are, respectively, slightly smaller and slightly larger than the corresponding values calculated on the donor layer of κ-(BDH-TTP)$_2$FeCl$_4$ (19.3 and 15.7×10^{-3} [31]), these values seem to be large enough to lead to 2D interaction similar to that in κ-(BDH-TTP)$_2$FeCl$_4$ with metallic conductivity to 1.5 K. Accordingly, it is at present difficult to rationalize the resistivity upturn observed around 5 K (Figure 15b). The arrangement of FeCl$_4^-$ anions is also similar to that in the paramagnetic κ-(BDH-TTP)$_2$FeCl$_4$ salt with $\theta = 0.041$ K, featuring the formation of pairs. The $Fe \cdots Fe$ distance within a pair [5.563(2) Å] is close to that in κ-(BDH-TTP)$_2$FeCl$_4$ [5.559(2) Å], whereas the shortest $Fe \cdots Fe$ distance between pairs [8.060(6) Å] is slightly shorter than that in κ-(BDH-TTP)$_2$FeCl$_4$ [8.169(2) Å], but yet would be too long to induce a direct interaction between the Fe moments. In addition, a superexchange mechanism via the Cl atoms would be deniable because the shortest $Cl \cdots Cl$ distance between the anions [3.578(4) Å] is close to that in κ-(BDH-TTP)$_2$FeCl$_4$ [3.594(2) Å]. However, the shortest $S \cdots Cl$ distance [3.602(5) Å] between the donor molecule and the FeCl$_4^-$ anion in κ-(DHOT-TTP)$_2$FeCl$_4$ is somewhat shorter than that in κ-(BDH-TTP)$_2$FeCl$_4$ [3.66(1) Å]. Eventually, it is likely that an interplay of the DHOT-TTP donor molecules and the FeCl$_4^-$ anions contributes to a very weak antiferromagnetic interaction observed in κ-(DHOT-TTP)$_2$FeCl$_4$ with $\theta = -0.50$ K.

The results above demonstrate that the DHOT-TTP donor molecules in κ-type salts have a cohesive force comparable to BDH-TTP. Our studies of the α- and κ-salts of DHDO-TTP suggest that the

replacement of one sulfur atom in BDH-TTP with oxygen holds the following two conflicting effects: (i) A decrease of overlap between donor molecules, which arises from a very small coefficient of HOMO on the oxygen atom, and (ii) an increase of chemical pressure caused by the oxygen atom smaller in size than the sulfur atom, which is reflected by a decrease of the unite cell volume as shown in Table 1, where the unit cell volumes of two isostructural series of α- and κ-salts of DHDO-TTP and BDH-TTP are summarized. It seems that both effects are in competition with each other in the κ-salts with orthogonal arrangement of donor dimers, whereas the former effect is preferentially exerted in columnar donor arrangements such as α-type packing mode in which the side-by-side interaction between donor molecules plays a crucial role in the formation of 2D interactions. Chemical modification combining the chalcogen substitution described here with the extension of σ-framework may lead to a fine-tuning of intermolecular interaction to develop new strongly correlated organic electron systems. We continue further studies along this line, one of which has been communicated in reference [47].
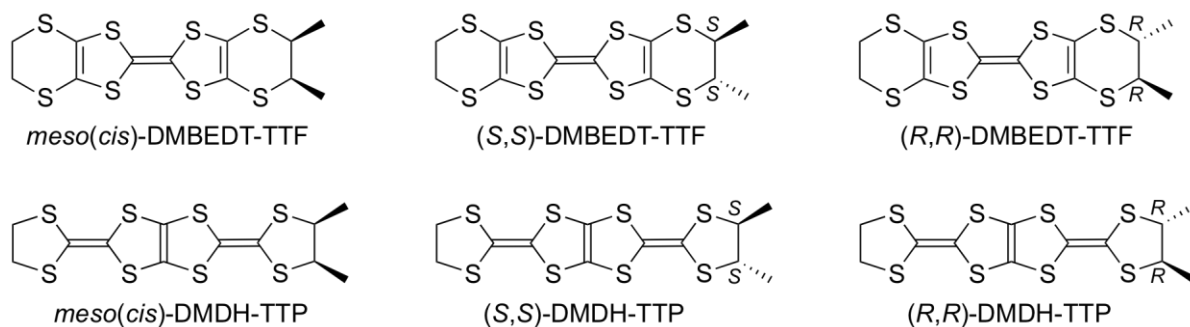
Table 1. Unit cell volumes of α- and κ-salts of DHOT-TTP and BDH-TTP.

	V (Å^3)
α-(DHOT-TTP)$_2$Au(CN)$_2$	1542.1(9)
α-(BDH-TTP)$_2$Au(CN)$_2$	1591(1)
κ-(DHOT-TTP)$_2$PF$_6$	3052(5)
κ-(DHOT-TTP)$_2$AsF$_6$	3070(2)
κ-(BDH-TTP)$_2$PF$_6$	3125.5(17)
κ-(DHOT-TTP)$_2$FeCl$_4$	3316(2)
κ-(BDH-TTP)$_2$FeCl$_4$	3379.1(8)

4. *Meso*-**DMDH-TTP Salts**

Our next research for the expansion of the σ-framework of BDH-TTP to control the electron correlation by decreasing the bandwidth involved the attachment of two methyl substituents in a vicinal manner to a terminal ethylene group of BDH-TTP. The syntheses of the corresponding dimethyl-substituted derivatives of BEDT-TTF, for which three kinds of stereoisomers, that is, a *meso* (or *cis*)-form (Figure 25) and an enantiomeric pair of (*R,R*)- and (*S,S*)-forms are possible, have been previously reported [48,49]. Zambounis *et al.* have found a superconducting salt of (*S,S*)-DMBEDT-TTF [1,2-dimethylethylenedithio(ethylenedithio)tetrathiafulvalene], κ-[(*S,S*)-DMBEDT-TTF]$_2$ClO$_4$ with T_c = 3 K (5 kbar) [50], and Kimura *et al.* reported the discovery of a superconducting salt of *meso*-DMBEDT-TTP, β-(*meso*-DMBEDT-TTF)$_2$PF$_6$ with T_c = 4.3 K (4.0 kbar) [49]. Similar to the case of DMBEDT-TTF, *meso*-, (*R,R*)- and (*S,S*)-forms exist as stereoisomers of DMDH-TTP [2-(4,5-dimethyl-1,3-dithiolan-2-ylidene)-5-(1,3-dithiolan-2-ylidene)-1,3,4,6-tetrathiapentalene]. We first attempted the synthesis of DMDH-TTP as a diastereomeric mixture of a *meso*-form and a *trans*-form (or racemate) containing equal numbers of (*R,R*)- and (*S,S*)-forms [51].

Figure 25. Stereoisomers of 1,2-dimethylethylenedithio(ethylenedithio)tetrathiafulvalene (DMBEDT-TTF) and 2-(4,5-dimethyl-1,3-dithiolan-2-ylidene)-5-(1,3-dithiolan-2-ylidene)-1,3,4,6-tetrathiapentalene (DMDH-TTP).

meso(*cis*)-DMBEDT-TTF   (*S*,*S*)-DMBEDT-TTF   (*R*,*R*)-DMBEDT-TTF

meso(*cis*)-DMDH-TTP   (*S*,*S*)-DMDH-TTP   (*R*,*R*)-DMDH-TTP

*4.1. Synthesis and Electrochemical Properties of DMDH-TTP*

The synthetic route to DMDH-TTP (Scheme 1) is essentially the same as that to BDH-TTP [15] except to use commercially available 2,3-butanedithiol **6** as a mixture of *meso*-, (*R*,*R*)- and (*S*,*S*)-forms instead of 1,2-ethanedithiol. Thus, the $BF_3 \cdot OEt_2$-mediated reaction of the dioxane-fused oxone **7** with **6** in CH_2Cl_2 gave oxone **8** with a dimethyl-substituted dithiolane ring in 94% yield as a 3.4:1 mixture of *meso*- and *trans*-dimethyl isomers. The ratio was determined by ^{1}H NMR integration for the methyl methine proton, and comparison with the ^{1}H NMR spectrum of (*S*,*S*)-**8**, prepared via the $BF_3 \cdot OEt_2$-meadiated reaction of **7** with (*S*,*S*)-**6** [52], ascertained that the minor product corresponds to the *trans*-isomer. Then, oxone **8** was converted to the corresponding tin dithiolate **9** by sequential treatment with MeMgBr and Cl_2SnBu_2 in THF followed by the Me_3Al-promoted reaction with ester **4** in CH_2Cl_2 to afford the coupling product **10** in 40% overall yield. Finally, DDQ oxidation of **10** in refluxing toluene furnished, after purification by silica gel chromatography followed by recrystallization, DMDH-TTP in 63%–70% yields in repeated experiments. The ^{1}H NMR spectrum showed two sets of signals to the methyl and methine protons, and the intensity rations for the two methine protons ranged from 3.7:1 to 4.7:1 in repeated experiments. Taking into account the *meso*-to-*trans* ration of **8**, it is most likely that the major isomer is *meso*-DMDH-TTP. The electrochemical behavior of the resulting DMDH-TTP was investigated by CV under the same conditions as used for the CV measurement of BDH-TTP (see Subsection 3.1). DMDH-TTP shows three reversible oxidation waves at 0.54, 0.81 and 1.36 V (*vs.* SCE). Both the values of E_1 (0.54 V) and ΔE ($E_2 - E_1$) (0.27 V) are somewhat smaller than those of BDH-TTP [$E_1 = 0.56$ V, ΔE ($E_2 - E_1$) = 0.29 V], indicating that the attachment of two methyl substituents causes a slight enhancement in the donor ability and a slight decrease in the on-site Coulomb repulsion due to an electron-donating effect of the methyl substituent.

Scheme 1. Synthetic route to DMDH-TTP.
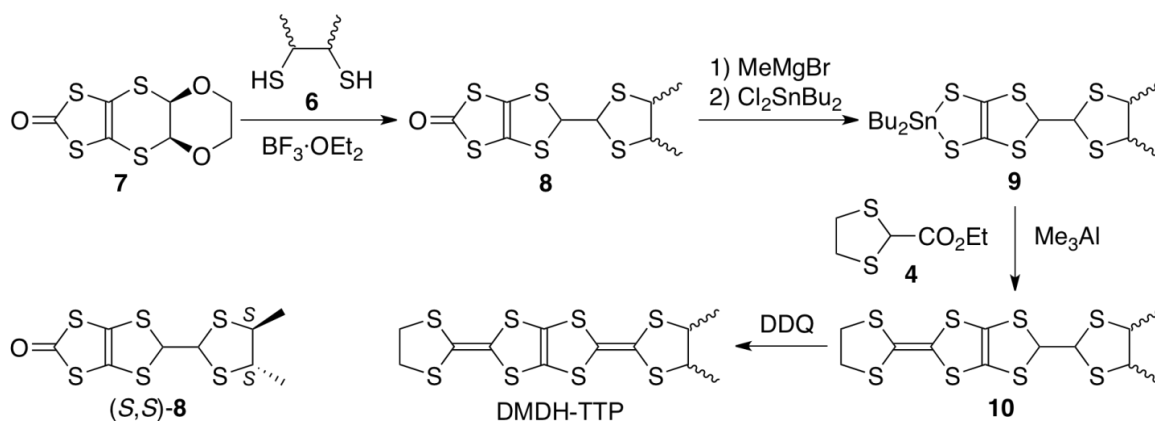
4.2. Preparation, Conductivity and Crystal and Electronic Structures of Meso-DMDH-TTP Salts

Controlled-current electrocrystallization [53,54] of a diastereomeric mixture of DMDH-TTP in 1,1,2-trichloroethane with n-Bu$_4$NX (X = AsF$_6$, PF$_6$ and BF$_4$) gave single crystals, together with other crystals of unsuitable quality or size for an X-ray structure determination [51,55]. Notably, the fact that all the single crystals contain only *meso*-DMDH-TTP as donor components with the composition (*meso*-DMDH-TTP)$_2$X (X = AsF$_6$, PF$_6$ and BF$_4$) was ascertained by X-ray analyses (*vide infra*), which is different from the report that electrocrystallization of a diastereomixture of the corresponding diethyl-substituted derivative of BEDT-TTP [2,5-bis(4,5-ethylenedithio-1,3-dithiol-2-ylidene)-1,3,4,6-tetrathiapentalene] with n-Bu$_4$NHgI$_3$ provides a single crystal of (Et$_2$BEDT-TTP)$_2$HgI$_3$ in which a donor stacking column consists of (*R,R*)-, (*S,S*)- and *meso* (or *cis*)-isomers [56]. Figure 26 shows the temperature dependence of the resistivities of the AsF$_6$ (σ_{rt} = 31 S cm^{-1}), PF$_6$ (σ_{rt} = 32 S cm^{-1}) and BF$_4$ (σ_{rt} = 54 S cm^{-1}) salts of *meso*-DMDH-TTP. Despite the presence of two methyl substituents in *meso*-DMDH-TTP, these salts maintained metallic conductivity down to a liquid helium temperature of 4.2 K, similar to the corresponding salts of BDH-TTP [15].

Figure 26. Temperature dependence of the resitivities for the AsF$_6$, PF$_6$ and BF$_4$ salts of *meso*-DMDH-TTP.
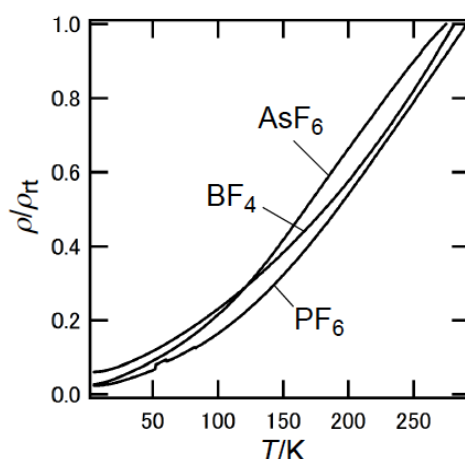
X-ray structural studies of the AsF$_6$ and PF$_6$ salts proved that their structures are isostructural with each other [55]. As shown in Figure 27a, the crystal structure of the AsF$_6$ salt contains two distinct types of donor layers, that is, a donor layer of the β-type (Figure 27b) and a donor layer of the β''-type (Figure 27c), which are interleaved by an anion layer. The asymmetric unit includes two crystallographically independent *meso*-DMDH-TTP molecules, both of which are, respectively, stacked in a head-to-tail manner to form the different donor layers. In the β-type donor layer, parallel stacks of somewhat dimerized donor molecules with separations of 3.61 and 3.78 Å occur along the *b*-axis, and intermolecular S ··S contacts close to or shorter than the van der Waals distance (3.70 Å) exist within a donor stack as well as between donor stacks. According to the overlap integrals calculated by the extended Hückel method, the values of the intrastack overlap integrals *p*1 and *p*2 and of the interstack overlap integral *q*1 are large, whereas the absolute value of the interstack overlap integral *a* along the crystallographic *a*-axis is smallest. This anisotropic interaction in the β-layer results in a 1D Fermi surface being open along the interstacking *a*-direction (Figure 27d). Meanwhile, the β''-type layer has donor stacks aligned along the [101] direction, and the donor stack contains *meso*-DMDH-TTP donor molecules alternating at almost the same separation of about 3.74 Å. Short S ··S contacts from 3.549(4) to 3.708(3) Å are observed between donor stacks rather than within a donor stack. Also the values of the interstack overlap integrals *q*1 and *q*2 are larger than those of the intrastack overlap integrals *p*1 and *p*2, leading to an open Fermi surface along the intrastaking [101] direction (Figure 27e). Although both the β- and β''-donor layers have 1D Fermi surfaces, the respective opening directions of the two 1D Fermi surfaces differ, so that the salt would exhibit metallic behavior down to a low temperature. These structural characteristics hold good in the case of the PF$_6$ salt. Such a dual-layered donor packing motif as found in β,β''-(*meso*-DMDH-TTP)$_2$X (X = AsF$_6$ and PF$_6$) has also occurred in the BDH-TTP salt, α'-(BDH-TTP)$_6$[Hg(SCN)$_3$][Hg(SCN)$_4$] [34], which features two different α'-types of donor layers responsible for two subsequent phase transitions, that is, a metal-semiconductor transition followed by a semiconductor-semiconductor transition. Furthermore, other examples of dual-layered conductors based on TTF donors have been reported [57].

On the other hand, the λ-type donor packing motif was found in the BF$_4$ salt of *meso*-DMDH-TTP (Figure 28a) [55]. The BF$_4^-$ anion has a large thermal motion around the boron atom and exhibits positional disorder of the fluorine atoms. The asymmetric unit contains two crystallographically discrete *meso*-DMDH-TTP molecules, which are stacked along the [011̄] direction in a head-to-tail manner with a four-folded period being 3.87, 3.75 and 3.61 Å apart. Intermolecular S ··S contacts shorter than the van der Waals distance (3.70 Å) are observed among three consecutive donor molecules in the four-fold period as well as between donor stacks (Figure 28b). Compared to the absolute values of the interstack overlap integrals *a*1, *a*2, *q*1, *q*2 and *q*3, larger absolute values are estimated for all the intrastack overlap integrals *p*1, *p*2 and *p*3. The tight-binding band calculation led to the energy dispersion curve and the Fermi surface shown in Figure 28c,d, respectively. Two highest bands are partially filled, and the Fermi surface associated with these bands contains a pair of wave-like lines and a closed rhombus-like loop centered at Γ. Thus, this salt has both 1D and 2D Fermi surfaces, and the 2D Fermi surface would cause the metallic conductivity down to 4.2 K.

Figure 27. (**a**) Crystal structure of (*meso*-DMDH-TTP)$_2$AsF$_6$. Interplanar distances in the β-type and β″-type donor layers are 3.61(*d*1), 3.78 (*d*2), 3.739 (*d*3) and 3.737 (*d*4) Å, respectively. (**b**) β-Type donor arrangement. Short S ⋅⋅S contacts [3.643(3)–3.710(2) Å] are shown by broken lines. Intermolecular overlap integrals *p*1, *p*2, *a*, *q*1 and *q*2 are 17.4, 11.4, −2.87, 12.0 and 4.43 × 10^{-3}, respectively. (**c**) β″-Type donor arrangement. Short S ⋅⋅S contacts [3.549(4)–3.708(3) Å] are drawn by broken lines. Intermolecular overlap integrals *p*1, *p*2, *a*, *q*1 and *q*2 are 4.66, 1.69, 3.80, 17.6 and 17.0 × 10^{-3}, respectively. (**d**) Band structure and Fermi surface of the β-type donor layer. (**e**) Band structure and Fermi surface of the β″-type donor layer (Reprinted with permission from reference 51, The Chemical Society of Japan.).
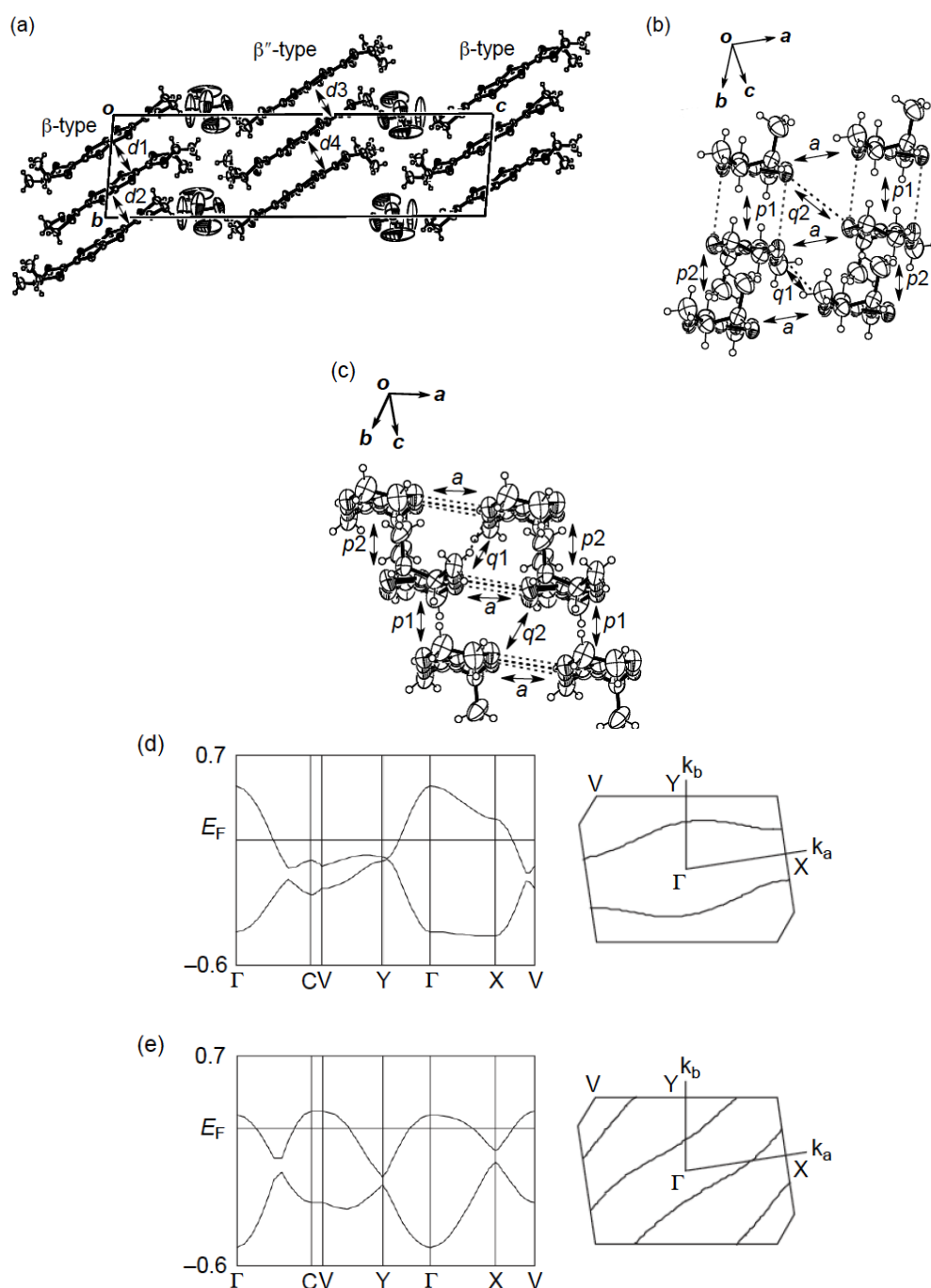
The donor stacking modes in β,β″-(*meso*-DMDH-TTP)$_2$X (X = AsF$_6$ and PF$_6$) and λ-(*meso*-DMDH-TTP)$_2$BF$_4$ are characterized as follows; (i) one methyl substituent in *meso*-DMDH-TTP is situated in an axial-like position almost perpendicular to the molecular plane including the π-electron system to relieve steric repulsion between the adjoining two methyl substituents and (ii) *meso*-DMDH-TTP donor molecules are stacked in a head-to-tail manner with formation of pairs in which two axial-like methyl substituents face each other; for instance, as seen in two *meso*-DMDH-TTP donor molecules with an interplanar spacing of 3.78 Å (*d*2) in the β-layer of β,β″-(*meso*-DMDH-TTP)$_2$AsF$_6$ (Figure 27a). It can be seen that donor stacking modes having these structural features cause the metallic state with the itinerant electron system. Therefore, a subtle chemical modification for altering these structural features would be required to control the electron correlation. To this end, we focused on a different stereochemistry between two methyl substituents, and accomplished the synthesis of a chiral DMDH-TTP, (*S*,*S*)-DMDH-TTP, and a racemic mixture of DMDH-TTP, (±)-DMDH-TTP, in both of which two methyl substituents are in a *trans* configuration. Preparation, conductivity measurements and structural studies of CT materials derived from (*S*,*S*)-DMDH-TTP and (±)-DMDH-TTP are currently in progress in our laboratory.

Figure 28. (**a**) Crystal structure of λ-(*meso*-DMDH-TTP)$_2$BF$_4$ viewed along the *a*-axis. Interplanar distances in a donor column are 3.87 (*d*1), 3.75 (*d*2) and 3.61 (*d*3) Å. (**b**) Donor arrangement in λ-(*meso*-DMDH-TTP)$_2$BF$_4$. Short S ··S contacts [3.583(5)–3.695(4) Å] are shown by broken lines. Intermolecular overlap integrals *p*1, *p*2, *p*3, *a*1, *a*2, *q*1, *q*2 and *q*3 are 15.5, −16.5, 14.7, −4.93, −5.35, 5.17, −9.66 and −6.63 × 10^{-3}, respectively. (**c**) Energy band structure of λ-(*meso*-DMDH-TTP)$_2$BF$_4$. (**d**) Fermi surfaces of λ-(*meso*-DMDH-TTP)$_2$BF$_4$. Wave-like lines are electron surfaces, whereas a closed rhombus-like loop is a hole surface (Reprinted with permission from reference 55, The Royal Society of Chemistry).
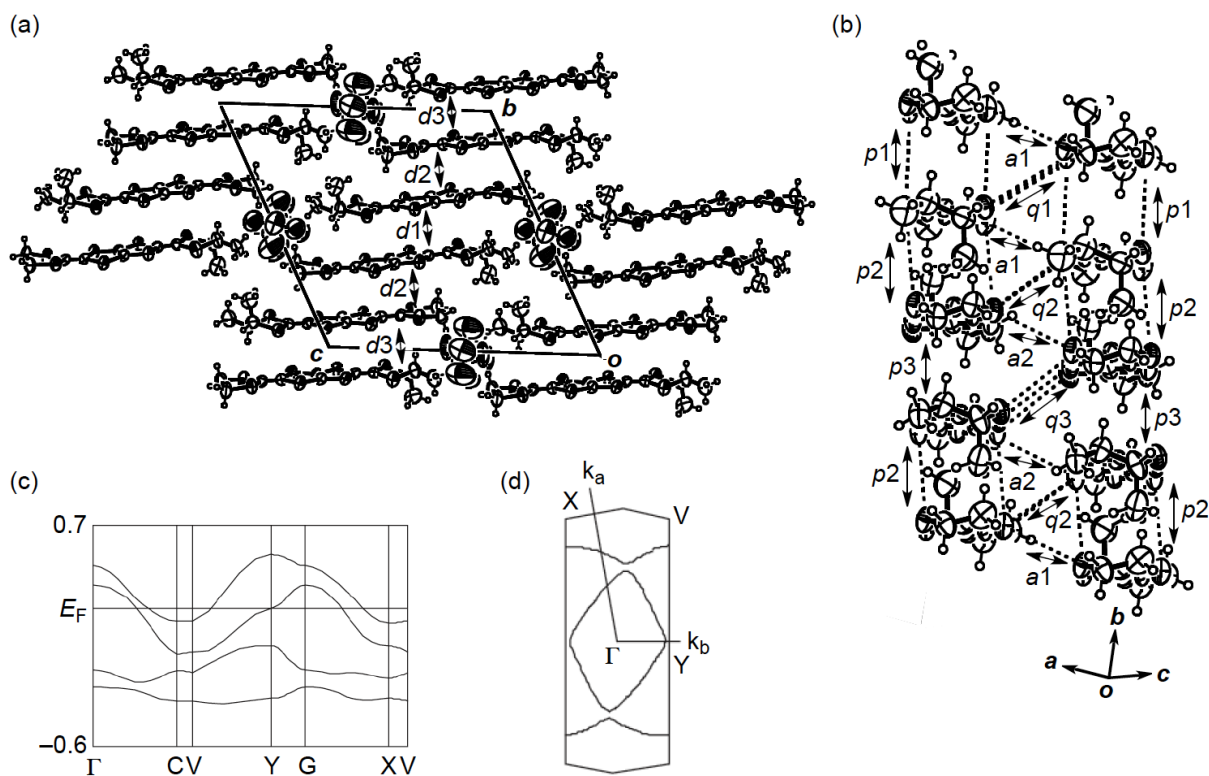
5. Conclusions

The molecular design of π-electron donors for obtaining molecular conductors with metallic conductivity has advanced in past years. We are now at the stage of designing π-donors for constructing strongly correlated organic electron systems. Organic molecular conductors with a strongly correlated electron system are undoubtedly attractive soft materials sensitive to the external stimuli as mentioned at the beginning of this review. Our approach described here relies on chemical modifications of BDH-TTP, and the molecular design based on such a control of electron correlation from the itinerant electron system should facilitate further production of π-donors with potential for novel strongly correlated electron systems. It is therefore an important subject of continued interest to reveal what chemical modification of BDH-TTP is effective in the construction of a new π-donor leading to the strongly correlated electron system. Simultaneously, it is hoped that our approach finds applications in other π-donors capable of forming CT materials with metallic conductivity arising from the itinerant electron system.

Acknowledgments

References and Notes

1. Ferraris, J.; Cowan, D.O.; Walatka, V., Jr.; Perlstein, J.H. Electron transfer in a new highly conducting donor-acceptor complex. *J. Am. Chem. Soc.* **1973**, *95*, 948–949.
2. Jérome, D.; Mazaud, A.; Ribault, M. Superconductivity in a synthetic organic conductor $(TMTSF)_2PF_6$. *J. Phys.* **1980**, *41*, L-95–L-98.
3. *TTF Chemistry–Fundamentals and Applications of Tetrathiafulvalene*; Yamada, J., Sugimoto, T., Eds.; Kodansha & Springer: Tokyo, Japan, 2004.
4. Molecular Conductors. In *Chemical Review*; Batail, P., Ed.; American Chemical Society: Washington, DC, USA, 2004.
5. Organic Conductors. In *Journal of the Physical Society of Japan*; Kagoshima, S., Kanoda, K., Mori, T., Eds.; The Physical Society of Japan (JPS): Tokyo, Japan, 2006.
6. Focus issue on organic conductors. In *Science and Technology of Advanced Materials*; Uji, S., Mori, T., Takahashi, T., Eds.; Elsevier: Amsterdam, The Netherlands, 2009.
7. Tajima, N.; Kajita, K. Experimental study of organic zero-gap conductor α-$(BEDT-TTF)_2I_3$. *Sci. Technol. Adv. Mater.* **2009**, *10*, 024308:1–024308:7.
8. Chollet, M.; Guerin, L.; Uchida, N.; Fukaya, S.; Shimoda, H.; Ishikawa, T.; Matsuda, K.; Hasegawa, T.; Ota, A.; Yamochi, H.; *et al.* Gigantic photoresponse in 1/4-filled-based organic salt $(EDO-TTF)_2PF_6$. *Science* **2005**, *307*, 86–89.

9. Sawano, F.; Terasaki, I.; Mori, H.; Mori, T.; Watanabe, M.; Ikeda, N.; Nogami, Y.; Noda, Y. An organic thyristor. *Nature* **2005**, *437*, 522–524.

10. Endo, H.; Kawamoto, T.; Mori, T.; Terasaki, I.; Kakiuchi, T.; Sawa, H.; Kodani, M.; Takimiya, K.; Otsubo, T. Current-induced metallic state in an organic (EDT-TSF)$_2$GaCl$_4$ conductor. *J. Am. Chem. Soc.* **2006**, *128*, 9006–9007.

11. Kanoda, K. Recent progress in NMR studies on organic conductors. *Hyperfine Interactions* **1997**, *104*, 235–249.

12. Yamada, J.; Nishikawa, H.; Kikuchi, K. Dihydro-TTFs and Bis-fused 1,3-Dithiol-2-ylidene Donors. In *TTF Chemistry–Fundamentals and Applications of Tetrathiafulvalene*; Yamada, J., Sugimoto, T., Eds.; Kodansha & Springer: Tokyo, Japan, 2004; Chapter 10, pp. 261–286.

13. Yamada, J. New approach to the achievement of organic superconductivity. *J. Mater. Chem.* **2004**, *14*, 2951–2953.

14. Yamada, J.; Akutsu, H.; Nishikawa, H.; Kikuchi, K. New trends in the synthesis of π-electron donors for molecular conductors and superconductors. *Chem. Rev.* **2004**, *104*, 5057–5083.

15. Yamada, J.; Watanabe, M.; Anzai, H.; Nishikawa, H.; Ikemoto, I.; Kikuchi, K. BDH-TTP as a structural isomer of BEDT-TTF, and its two-dimensional hexafluorophosphate salt. *Angew. Chem. Int. Ed.* **1999**, *38*, 810–813.

16. Yamada, J.; Watanabe, M.; Akutsu, H.; Nakatsuji, S.; Nishikawa, H.; Ikemoto, I.; Kikuchi, K. New organic superconductors β-(BDA-TTP)$_2$X [BDA-TTP = 2,5-bis(1,3-dithian-2-ylidene)-1,3,4,6-tetrathiapentalene; X$^-$ = SbF$_6$$^-$, AsF$_6$$^-$, and PF$_6$$^-$]. *J. Am. Chem. Soc.* **2001**, *123*, 4174–4180.

17. Yamada, J.; Toita, T.; Akutsu, H.; Nakatsuji, S.; Nishikawa, H.; Ikemoto, I.; Kikuchi, K.; Choi, E.S.; Graf, D.; Brooks, J.S. A new organic superconductor, β-(BDA-TTP)$_2$GaCl$_4$ [BDA-TTP = 2,5-bis(1,3-dithian-2-ylidene)-1,3,4,6-tetrathiapentalene]. *Chem. Commun.* **2003**, 2230–2231.

18. Choi, E.S.; Graf, D.; Brooks, J.S.; Yamada, J.; Akutsu, H.; Kikuchi, K.; Tokumoto, M. Pressure-dependent ground states and fermiology in β-(BDA-TTP)$_2$MCl$_4$ (M = Fe, Ga). *Phys. Rev. B* **2004**, *70*, 024517:1–024517:8.

19. Williams, J.M.; Ferraro, J.R.; Thorn, R.J.; Carlson, D.; Geiser, U.; Wang, H.H.; Kini, A.M.; Whangbo, M.-H. *Organic Superconductors (Including Fullerenes): Synthesis, Structure, Properties, and Theory*; Prentice Hall: Englewood Cliffs, NJ, USA, 1992.

20. Yamada, J.; Fujimoto, K.; Akutsu, H.; Nakatsuji, S.; Miyazaki, A.; Aimatsu, M.; Kudo, S.; Enoki, T.; Kikuchi, K. Pressure effect on the electrical conductivity and superconductivity of β-(BDA-TTP)$_2$I$_3$. *Chem. Commun.* **2006**, 1331–1333.

21. Kikuchi, K.; Isono, T.; Kojima, M.; Yoshino, H.; Kodama, T.; Fujita, W.; Yokogawa, K.; Yoshino, H.; Murata, K.; Kaihatsu, T.; Akutsu, H.; Yamada, J. Uniaxial strain orientation dependence of superconducting transition temperature (T_c) and critical superconducting pressure (P_c) in β-(BDA-TTP)$_2$I$_3$. *J. Am. Chem. Soc.* **2011**, *133*, 19590–19593.

22. Mori, T.; Kobayashi, A.; Sasaki, Y.; Kobayashi, H.; Saito, G.; Inokuchi, H. The intermolecular interaction of tetrathiafulvalene and bis(ethylenedithio)tetrathiafulvalene in organic metals. Calculation of orbital overlaps and models of energy-band structures. *Bull. Chem. Soc. Jpn.* **1984**, *57*, 627–633.

23. Seo, H.; Hotta, C.; Fukuyama, H. Toward systematic understanding of diversity of electronic properties in low-dimensional molecular solids. *Chem. Rev.* **2004**, *104*, 5005–5036.

24. Miyagawa, K.; Kanoda, K.; Kawamoto, A. NMR studies on two-dimensional molecular conductors and superconductors: Mott transition in κ-(BEDT-TTF)$_2$X. *Chem. Rev.* **2004**, *104*, 5635–5653.

25. Mori, H.; Tanaka, S.; Mori, T. Systematic study of the electronic state in θ-type BEDT-TTF organic conductors by changing the electronic correlation. *Phys. Rev. B* **1998**, *57*, 12023–12029.

26. Nishikawa, H.; Sato, Y.; Kikuchi, K.; Kodama, T.; Ikemoto, I.; Yamada, J.; Oshio, H.; Kondo, R.; Kagoshima, S. Charge ordering and pressure-induced superconductivity in β″-(DODHT)$_2$PF$_6$. *Phys. Rev. B* **2005**, *72*, 052510:1–052510:4.

27. Kagoshima, S.; Kondo, R. Control of electronic properties of molecular conductors by uniaxial strain. *Chem. Rev.* **2004**, *104*, 5593–5608.

28. Murata, K.; Kagoshima, S.; Yasuzuka, S.; Yoshino, H.; Kondo, R. High-pressure research in organic conductors. *J. Phys. Soc. Jpn.* **2006**, *75*, 051015:1–051015:15.

29. Uruichi, M.; Nakano, C.; Tanaka, M.; Yakushi, K.; Kaihatsu, T.; Yamada, J. Infrared and Raman spectroscopic study of BDA-TTP [2,5-bis(1,3-dithian-2-ylidene)-1,3,4,6-tetrathiapentalene] and its charge-transfer salts. *Solid State Commun.* **2008**, *147*, 484–489.

30. Kanoda, K. Metal-insulator transition in κ-(ET)$_2$X and (DCNQI)$_2$M: Two contrasting manifestation of electron correlation. *J. Phys. Soc. Jpn.* **2006**, *75*, 051007:1–051007:16.

31. Kikuchi, K.; Nishikawa, H.; Ikemoto, I.; Toita, T.; Akutsu, H.; Nakatsuji, S.; Yamada, J. Tetrachloroferrare (III) salts of BDH-TTP [2,5-bis(1,3-dithiolan-2-ylidene)-1,3,4,6-tetrathiapentalene] and BDA-TTP [2,5-bis(1,3-dithian-2-ylidene)-1,3,4,6-tetrathiapentalene]: Crystal structures and physical properties. *J. Solid State Chem.* **2002**, *168*, 503–508.

32. Yamada, J. A new approach in the design of organic superconductors. *J. Phys. IV Fr.* **2004**, *114*, 439–443.

33. Shevyakova, I.; Buravov, L.; Tkacheva, V.; Zorina., L.; Khasanov, S.; Simonov, S.; Yamada, J.; Canadel, E.; Shibaeva, R.; Yagubskii, E. New organic metals based on BDH-TTP radical cation salts with the photochromic nitroprusside anion [FeNO(CN)$_5$]$^{2-}$. *Adv. Funct. Mater.* **2004**, *14*, 660–668.

34. Kushch, N.D.; Kazakova, A.V.; Buravov, L.I.; Yagubskii, E.B.; Simonov, S.V.; Zorina, L.V.; Khasanov, S.S.; Shibaeva, R.P.; Canadell, E.; Son, H.; Yamada, J. The first BDH-TTP radical cation salts with mercuric counterions, κ-(BDH-TTP)$_4$[Hg(SCN)$_4$] C$_6$H$_5$NO$_2$ and α′-(BDH-TTP)$_6$[Hg(SCN)$_3$][Hg(SCN)$_4$]. *Synth. Met.* **2005**, *155*, 588–594.

35. Zhilyaeva, E.I.; Flakina, A.M.; Lyubovskaya, R.N.; Fedyanin, I.V.; Lyssenko, K.A.; Antipin, M.Y.; Lyubovskii, R.B.; Yudanova, E.I.; Yamada, J. Synthesis, crystal structures and properties of new radical cation salts based on some tetrathiapentalene derivatives with halogenomercurate anions. *Synth. Met.* **2006**, *156*, 991–998.

36. Kushch, N.D.; Kazakova, A.V.; Buravov, L.I.; Yagubskii, E.B.; Simonov, S.V.; Zorina, L.V.; Khasanov, S.S.; Shibaeva, R.P.; Yamada, J.; Umemiya, M. New molecular magnetic metals: κ-(BDH-TTP)$_4$CuCl$_4$ (H$_2$O)$_n$ and κ-(BDH-TTP)$_2$[CuCl$_4$]$_{0.67}$ (H$_2$O)$_{0.33}$ (BDH-TTP is 2,5-bis(1,3-dithiolan-2-ylidene)-1,3,4,6-tetrathiapentalene). *Russ. Chem. Bull. Int. Ed.* **2010**, *59*, 1–6.

37. Misaki, Y. Tetrathiapentalene-based organic conductors. *Sci. Technol. Adv. Mater.* **2009**, *10*, 024301:1–02430122:7.

38. Moge, M.; Hellberg, J.; Törnroos, K.W.; von Schütz, J.-U. Synthesis and crystal structure of a new unsymmetrical oxygen containing TTF. *Adv. Mater.* **1996**, *8*, 807–808.

39. Yamada, J.; Kunigita, K.; Akutsu, H.; Nakatsuji, S.; Kikuchi, K. Monooxygen-containing analogue of BDH-TTP, DHOT-TTP [2-(1,3-dithiolan-2-ylidene)-5-(1,3-oxathiolan-2-ylidene)-1,3,4,6-tetrathiapentalene], and its metallic AuI$_2$ salt. *Chem. Lett.* **2005**, *34*, 32–33.

40. Yamada, J.; Kunigita, K.; Akutsu, H.; Nakatsuji, S.; Kikuchi, K. Competitive effect in metallic κ-type DHOT-TTP [2-(1,3-dithiolan-2-ylidene)-5-(1,3-oxathiolan-2-ylidene)-1,3,4,6-tetrathiapentalene] salts. *Chem. Lett.* **2005**, *34*, 1126–1127.

41. Yamada, J.; Oka, R.; Mangetsu, T.; Akutsu, H.; Nakatsuji, S.; Nishikawa, H.; Ikemoto, I.; Kikuchi, K. Tetrathiafulvalene derivatives linking a dichalcogenolane ring through the σ-bond: New donor molecules for organic metals. *Chem. Mater.* **2001**, *13*, 1770–1777.

42. Kini, A.M.; Mori, T.; Geiser, U.; Budz, S.M.; Williams, J.M. 4,5-Ethylenedioxy-4,5'-ethylenedithiotetrathiafulvalene (EOET): A new unsymmetrical electron donor. *J. Chem. Soc. Chem. Commun.* **1990**, 647–648.

43. Yamada, J.; Kunigita, K.; Akutsu, H.; Nakatsuji, S.; Kikuchi, K. Department of Material Science, Graduate School of Material Science, University of Hyogo, 3-2-1 Kouto, Kamigori-cho, Ako-gun, Hyogo 678-1297, Japan. Unpublished work, 2012.

44. Crystal data for (BDH-TTP)$_2$AuI$_2$: C$_{10}$H$_8$Au$_{0.50}$IS$_8$, M = 610.04, triclinic, space group $P\bar{1}$, a = 4.9044(18), b = 5.581(3), c = 15.543(6) Å, α = 99.157(9)°, β = 91.500(10)° γ = 91.779(11)°, V = 419.6(3) Å^3, Z = 1, T = 294 K, D_{calcd} = 2.414 g cm^{-3}, R = 0.0697 and R_w = 0.2406 for 1329 observed reflections with $I > 2.0\sigma(I)$ from 1840 unique reflections. The crystal structure has been deposited at the Cambridge Crystallographic Data Centre (CCDC 885998).

45. Crystal data for α-(DHOT-TTP)$_2$Au(CN)$_2$: C$_{22}$H$_{16}$AuN$_2$O$_2$S$_{14}$, M = 986.19, triclinic, space group $P\bar{1}$, a = 11.295(4), b = 17.069(5), c = 8.579(4) Å, α = 90.92(3)°, β = 110.04(3)° γ = 96.21(3)°, V = 1542.1(10) Å^3, Z = 2, T = 297 K, D_{calcd} = 2.124 g cm^{-3}, R = 0.0571 and R_w = 0.1773 for 5419 observed reflections with $I > 2.0\sigma(I)$ from 7083 unique reflections. The crystal structure has been deposited at the Cambridge Crystallographic Data Centre (CCDC 885999).

46. Crystal data for α-(BDH-TTP)$_2$Au(CN)$_2$: C$_{22}$H$_{16}$AuN$_2$S$_{16}$, M = 1018.31, triclinic, space group $P\bar{1}$, a = 11.601(5), b = 17.141(9), c = 8.570(3) Å, α = 92.21(4)°, β = 110.01(3)°, γ = 95.04(4)°, V = 1591(1) Å^3, Z = 2, T = 299.2 K, D_{calcd} = 2.126 g cm^{-3}, R = 0.0672 and R_w = 0.0668 for 5216 observed reflections with $I > 3.00\sigma(I)$ from 7330 unique reflections. The crystal structure has been deposited at the Cambridge Crystallographic Data Centre (CCDC 885997).

47. Yamada, J.; Hiratani, N.; Kunigita, K.; Akutsu, H.; Nakatsuji, S.; Kikuchi, K. Monooxygen-containing Analogues of DHDA-TTP, DHOTA-TTP and OTDA-TTP, and Their Charge-transfer Salts. In *Multifunctional Conducting Molecular Materials*; Saito, G., Wudl, F., Haddon, R.C., Tanigaki, K., Enoki, T., Katz, H.E., Maesato, M., Eds.; RSC Publishing: Cambridge, UK, 2007; pp. 67–70.

48. Matsumiya, S.; Izuoka, A.; Sugawara, T.; Taruishi, T.; Kawada, Y. Effect of methyl substitution on conformation and molecular arrangement of BEDT-TTF derivatives in the crystalline environment. *Bull. Chem. Soc. Jpn.* **1993**, *66*, 513–522.

49. Kimura, S.; Maejima, T.; Suzuki, H.; Chiba, R.; Mori, H.; Kawamoto, T.; Mori, T.; Moriyama, H.; Nishio, Y.; Kajita, K. A new organic superconductor β-(*meso*-DMBEDT-TTF)$_2$PF$_6$. *Chem. Commun.* **2004**, 2454–2455.

50. Zambounis, J.S.; Mayer, C.W.; Hauenstein, K.; Hilti, B.; Hofherr, W.; Pfeiffer, J. Crystal structure and electrical properties of κ-((*S,S*)-DMBEDT-TTF)$_2$ClO$_4$. *Adv. Mater.* **1992**, *4*, 33–35.

51. Yamada, J.; Song, H.; Akutsu, H.; Nakatsuji, S.; Kikuchi, K. Synthesis of dimethyl-substituted BDH-TTP derivative DMDH-TTP as a diastereomeric mixture, and the formation of metallic salts involving only *meso*-DMDH-TTP. *Chem. Lett.* **2005**, *34*, 1404–1405.

52. Corey, E.J.; Mitra, R.B. L(+)-2,3-butanedithiol: Synthesis and application to the resolution of racemic carbonyl compounds. *J. Am. Chem. Soc.* **1962**, *84*, 2938–2941.

53. Anzai, H.; Delrieu, J.M.; Takasaki, S.; Nakatsuji, S.; Yamada, J. Crystal growth of organic charge-transfer complexes by electrocrystallization with controlled applied current. *J. Cryst. Growth* **1995**, *154*, 145–150.

54. Nishikawa, H.; Sato, T.; Kodama, T.; Ikemoto, I.; Kikuchi, K.; Anzai, H.; Yamada, J. Electrical properties and crystal structures of metallic TMVT salts. *J. Mater. Chem.* **1999**, *9*, 693–696.

55. Yamada, J.; Song, H.; Akutsu, H.; Nakatsuji, S.; Kikuchi, K. Dimethyl-substituted Analogue of BDH-TTP, DMDH-TTP, and Its Metallic Salts. In *Multifunctional Conducting Molecular Materials*; Saito, G., Wudl, F., Haddon, R.C., Tanigaki, K., Enoki, T., Katz, H.E., Maesato, M., Eds.; RSC Publishing: Cambridge, UK, 2007; pp. 63–66.

56. Kimura, S.; Hanazato, S.; Kurai, H.; Mori, T.; Misaki, Y.; Tanaka, K. Stereochemically ordered donor columns in an organic conductor, (Et$_2$BEDT-TTP)$_2$HgI$_3$. *Tetrahedron Lett.* **2001**, *42*, 5729–5732.

57. Schlueter, J.A.; Wiehl, L.; Park, H.; de Souza, M.; Lang, M.; Koo, H.-J.; Whangbo, M.-H. Enhanced critical temperature in a dual-layered molecular superconductor. *J. Am. Chem. Soc.* **2010**, *132*, 16308–16310, and references therein.